Efficient Wireless Charging with Gallium Nitride FETs
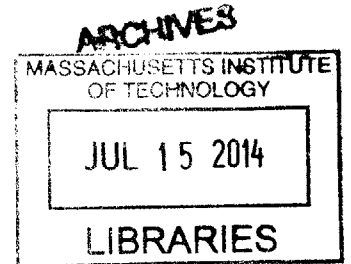
by

Theresa Yeh

Submitted to the Department of Electrical Engineering and Computer Science in
partial fulfillment of the requirements for the degree of

Masters of Engineering

in

Electrical Engineering and Computer Science

at the Massachusetts Institute of Technology

June 2014

© 2014 Massachusetts Institute of Technology
All Rights Reserved.

Signature of Author: ___ Signature redacted _____

Department of Electrical Engineering and Computer Science

May 23, 2014

Signature redacted

Certified by: _____

Anantha Chandrakasan, Joseph F. and Nancy P. Keithley Professor of EECS

Thesis Supervisor

Signature redacted

Certified by: _____ _____

Tomás Palacios, Professor of EECS

Thesis Supervisor

Signature redacted

Accepted by: _____ _____

Albert Meyer, Professor of Electrical Engineering

Chairman, Masters of Engineering Thesis Committee

Efficient Wireless Charging with Gallium Nitride FETs

by Theresa Yeh

Submitted to the Department of Electrical Engineering
and Computer Science on May 23, 2014
in Partial Fulfillment of the Requirements for the Degree
of Masters of Engineering in Electrical Engineering and Computer Science

Abstract

Though wireless charging is more convenient than traditional wired charging methods, it is currently less efficient. This not only wastes power but can also result in a longer charging time. Improving the efficiency of wireless charging systems is equivalent to reducing the sources of loss in the system. In this work, we focus on losses originating from the transistor. Resonant inductive wireless charging systems were designed and implemented for efficiency comparisons. We show in our experiments that replacing the traditional Silicon MOSFET with a Gallium Nitride FET can increase the overall system efficiency by 5%.

Thesis Co-Advisors: Anantha Chandrakasan & Tomás Palacios
Title: Professors of Electrical Engineering and Computer Science

Acknowledgments

I would like to thank my co-advisors, Anantha Chandrakasan and Tomás Palacios, for their guidance, encouragement, and generous support. I would like to thank Anantha for giving me the opportunity to be a SuperUROP in his group during my senior year and continuing on as a M.Eng. I would also like to thank Tomás for his guidance and insight this past year. My project has taught me many practical skills and gave me exposure to various applications of electrical engineering. Their dedication to research and willingness to help their students made them the perfect co-advisers.

I would like to thank Nachiket Desai for his guidance and patience throughout my M.Eng. year. He is always very willing to listen to my research challenges and discuss potential ideas and solutions. I have learned a lot from him and really appreciate his help. I have also been very fortunate to have had the opportunity to interact with some of the most intelligent people in MTL/RLE during my time at MIT.

Likewise, many thanks go out to Jing Kong and Khurram Afridi for being such great professors and sources of inspiration and encouragement during my time at MIT.

I would also like to thank all my friends from MIT and from home. I would not be where I am today without their support. These past five years at MIT together have been an amazing journey that I will always cherish. Lastly, I am forever grateful for my family. They have always encouraged me to challenge myself and helped me along the way. All my successes would not have been possible without the support of others.

Contents

List of Figures

List of Tables

Chapter 1

Introduction

■ 1.1 Motivation

Wireless transfer of power and signals over distances has been rapidly growing. The ability to transfer energy from one device to another without cables improves the convenience for consumers. Wireless technology can be used in a wide variety of applications such as cellphones, game controllers, laptops, robots, electric vehicles, digital photo frames, biomedical implants, and many more. Consumers who use this hands-free system no longer need to carry around multiple cables or worry about contaminants getting into their devices.

There are two types of wireless power transfer: far-field and near-field. Far-field power transfer uses RF antennas or lasers to transmit over long distances. Thus, power is radiated out. In contrast, near-field power uses localized electric or magnetic fields coupled between TX and RX over short and medium distances for reactive power [26].

This thesis will focus on near-field power transfer for .25 inch up to 1 inch for a device people use either their daily lives: cellphones. Currently, there are two main concerns that cause consumers to revert back to traditional charging methods.

One disadvantage is that not all cellphones currently have the capability to support the wireless charging technology. Consumers need to buy phone cases that have the necessary built-in technology inside. However, as wireless charging technology expands and matures, this issue can be resolved by manufacturers incorporating the necessary technology into cellphones directly at a small increase in cost. Another concern for consumers is the increase in charging time and power consumption when wireless charging their cellphones.

This thesis will examine and develop a further understanding of wireless charging technology in order to improve the system. Currently, the losses in various conversion
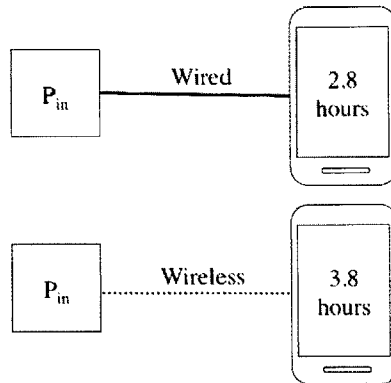
Figure 1.1: Comparison of Charging Times between Wired and Wireless Charger for Samsung Galaxy S4 with same input power

circuits of the wireless charger limit the efficiency and charging rate. Wireless charging takes about 35% longer to charge cellphones than traditional cellphone charging methods when given the same input power because of increasing inefficiencies [16]. As shown in Figure 1.1, to fully charge the Galaxy S4 normally takes a little less than three hours. However, a wireless Samsung Qi charger increases the charging time to almost four hours. Qi is an interface standard developed by the Wireless Power Consortium for inductive electrical power transfer over distances of up to 4 cm (1.6 inches) [21]. In order to maintain a shorter charging time, more power consumption is necessary. Since inefficient chargers waste more power, extra circuitry and cost is necessary to remove the excess heat.

To reduce power consumption and charging time, the efficiency of the conversion circuits needs to be improved. Though there are many sources of loss in each stage, losses from the transistor will be the focus for this thesis. This thesis will evaluate the potential efficiency gain of the overall wireless charging system when replacing a traditional Silicon MOSFET with a Gallium Nitride FET.

■ 1.1.1 Goal

State of the art wireless chargers are up to 80% efficient for short distances between the charger (transmitter) and device (receiver) [15]. The goal of this thesis is to design and implement two wireless charging systems with different transistors for overall efficiency

comparison. One board will utilize the traditional Silicon MOSFET. The other board will replace the MOSFET with a Gallium Nitride FET (GaNFET), while keeping the circuitry and components as consistent as possible. The systems should have flexibility in alignment between the device delivering and receiving power. The differences between the two contrasting systems should be understood and analyzed. Finally, the charging system should demonstrate successful power transfer through two demos: powering an LED demo board and a cellphone.

■ 1.1.2 Thesis Overview

This thesis discusses the design choices made, implementation, and findings between the two systems. After understanding existing wireless charging technology and the benefits of GaNFETs, inductor coils were first designed and implemented. Then, different converter topologies for the transmitter and receiver units were explored. The next step was to find the optimal components for the desired architectures to maximize the system end-to-end efficiency. Results and analysis between the two systems are discussed. Then, successful power transfer demos with the implemented wireless charging systems are demonstrated. Discussion of layout, testing techniques, higher frequency system, and future work is also explained.

Chapter 2

Existing Technology

■ 2.1 Background

■ 2.1.1 GaNFET versus. MOSFET

Gallium Nitride FETs (GaNFETs) are transistors with similar properties as Silicon MOSFETs. Though Gallium Nitride technology is still developing, there are already many benefits for various applications [4]. Table 2.1 compares some of the keys parameters between MOSFETs and GaNFETs that are both rated for 200V and 3A.

The main figure of merit (FOM) is $R_{ds,on} \times Q_G$. This FOM for GaNFETs is much lower than that for MOSFETs [17]. Thus, there is the potential for GaNFETs to dissipate less power than MOSFETs in switching converters. In addition, a lower $Q_G \times R_{ds,on}$ product allows the GaNFET to switch faster leading to a smaller overall converter size. Another advantage is that GaNFETs also have ultra-small package footprints which saves space for higher density power converters [28]. As research in Gallium Nitride continues to expand, the GaNFETs available in the future market should maintain the lower parasitics but increase the breakdown voltages at a similar cost to Silicon MOSFETs [10]. Wireless charging is just one of the many applications that the benefits of Gallium Nitride technology.

Table 2.1: GaNFET vs. MOSFET[9] [11]

Switch	$V_{DSS}(V)$	$I_D(A)$	$R_{dson}(\text{m}\Omega)$	$C_{iss}(\text{pF})$	$C_{oss}(\text{pF})$	$Q_G(nC)$
GaNFET	200	3	90	130	90	1.8
MOSFET	200	3	130	1300	250	18

■ 2.1.2 Wireless Charging Technology: Three Approaches

There are three general wireless charging approaches: infrared, radio frequencies (RF), and inductive. One requirement when using infrared is that there needs to be a direct pathway from the transmitter to object receiving power. If there are any obstacles between the objects, then the power transfer will not work. Another approach is to transfer energy wirelessly through radio frequencies. However, under far-field situations, this can induce strong electric fields that would trigger safety concerns [18] . People can experience static shocks when coming in contact with objects with strong electric fields [7]. Thus, the best option for charging cellphones wirelessly is some form of inductive charging. Inductive charging is a safe option because the magnetic fields generated by the alternating currents do not affect human tissue like electric fields do [18]. However, at extremely high magnetic fields, faint flickering visual sensations and muscles stimulations can potentially occur [7]. Thus, it is still important to keep in mind the amount of fields coming from the charging system.

■ 2.1.3 Inductive Charging

Traditional inductive charging methods use one primary coil to induce a magnetic field that couples onto a secondary coil, so a portion of the input power can be converted into useful electrical current to charge the output device [6]. The basic structure of an inductive charging system is shown in Figure 2.1.

The transmitter and receiver sides are electrically isolated. The transmitter side consists of a DC/AC converter which includes the primary coil. Once given a supply voltage to power the circuitry, an alternating current runs through the primary coil that induces a fluctuating magnetic field which is picked up by the secondary coil. The receiver side rectifies and converts the AC current into a DC voltage that can be delivered to the load.

■ 2.1.4 Coupling Coefficients

Depending on the distance, alignment, shape, and angles between the primary and secondary coil, the secondary coil absorbs different amounts of the magnetic flux generated from the primary side as shown in Figure 2.2. Magnetic field density decreases as distance between the coils increase. The coupling coefficient (k) gives a relative measure of how much magnetic flux generated is actually coupled onto receiver coil. Coupling
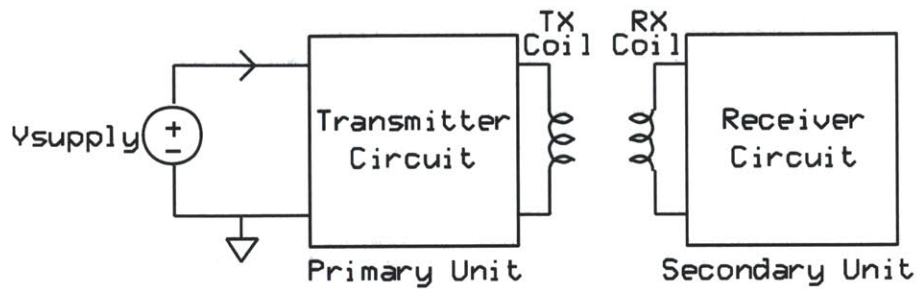
Figure 2.1: Inductive Charging System
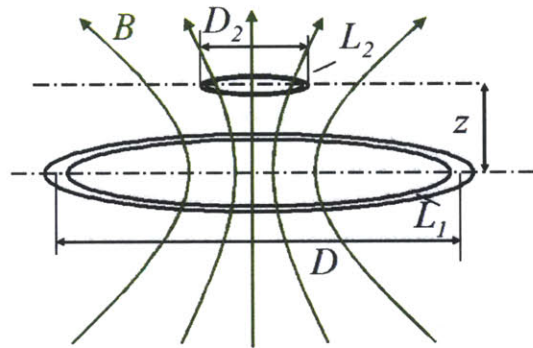
Figure 2.2: Inductive Coupled Power Transfer [26]

coefficients can range from 0 where is no flux received to 1 where all the flux generated is also received.

In this thesis, the coupling factors range from .03 at 2 inches to .11 at 0 cm between the coils. High coupling coefficients are more difficult to achieve when there is flexibility for misalignment between the TX and RX coil. A comparison between simulated and actual k values are shown in the Chapter 5. Since there is a strong dependency of efficiency on k, the secondary coil should be as tightly coupled to the primary coil as possible to maximize efficiency.

■ 2.2 Previous Work: Inductive Resonant Charging

In order to allow for obstacles, misalignment, and transferring power over small to medium distances, traditional inductive charging is not sufficient. Traditional inductive
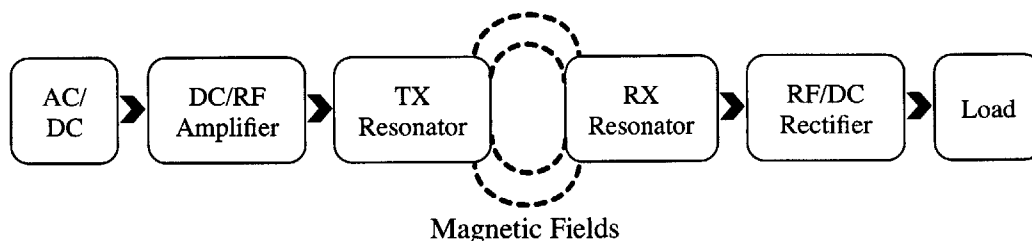
Figure 2.3: Magnetic Resonance Charging System Overview

charging requires high coupling coefficients between the primary and secondary coil to overcome impedance mismatch between inductive coil and resistive load, which limits the flexibility of the system. However, the limitations can be overcome by resonating out the coil inductance with a capacitor.

The difference between the two methods is that traditional charging requires the power source and capture device to be very close to one another for efficient power transfer, whereas magnetic resonant charging allows for more flexibility. Many traditional inductive charging solutions require a cradle to hold the capture device, or a mat on which the capture device must rest such as a electric toothbrush. Currently, WiTricity's wireless charging technology incorporates strong resonant coupling, which allows for power to be transferred efficiently even when the distances between the power source and capture device are several times the size of the devices themselves [15]. With resonant inductive charging, WiTricity has shown the ability to transfer power from one device to another up to a few meters with high quality factor coils almost at a 40% efficiency [15].

Resonance can be added to the existing system for efficient power transfer by forming LC tanks on both the primary and secondary side of the system. For optimal power transfer, the two LC tanks should be tuned to the same resonant frequency where there is weak energy coupling with off-resonant objects [3]. Both resonators should have low loss components and a narrow resonant frequency width (high Q) [18]. In this thesis, both LC tanks are tuned to approximately the switching frequency at 6.78MHz. The switching frequency and implementation of the system is discussed in more detail in later chapters. The general block diagram for a magnetic resonance charging system is shown in Figure 2.3.

■ 2.3 Identifying Sources of Loss

The most significant sources of loss in an inductive charging system are from the non-idealities of the inductor coils, rectifier, and transistor. There has been considerable amounts of research focused on the transmitter and receiver charging coils in terms of shapes, orientations, and other parameters. However, there are also other sources of losses that limit the efficiency of the wireless charger as well. In this thesis, the first goal is to understand the sources of loss and how they vary under different conditions. After gaining better insight on the losses, the second goal is to determine if there is improvement in efficiency by replacing the traditional transistor used in the system.

■ 2.4 Sources of Losses

■ 2.4.1 Transmitter Side Losses

Inductor Losses

A lumped model of a real inductor is an ideal L in series with R, parallel with a lumped C as shown in Figure 2.4.

Coils Losses

The coils are air core inductors. At high frequencies, they suffer from high resistances because of the following effects: skin effect and proximity effect [12]. The cross sectional area of the wire is no longer used to conduct current at high frequencies. Instead, current travels along the surface of the wire which increases the effective resistance of the coils. Proximity effect has a similar outcome and occurs when parallel wires are close to each other. Thus, the AC current running through the wire dissipates power. The AC Resistance (ACR) Loss can be calculated by:

ACR Loss:

$$P_{acr} = I_{rms}^2 \times R_{eff} \tag{2.1}$$

RF choke Losses

Ferromagnetic-core inductors such as the a RF choke (RFC) use a magnetic core to allow for high inductance values. Chokes are designed to limit the AC current and let DC current pass. The DC Resistance (DCR) loss is due to current passing through the intrinsic DC resistance in the RFC. There is also core losses due the the time-varying
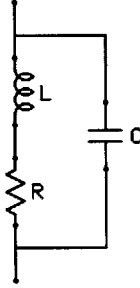
Figure 2.4: Inductor Model

magnetic field in the core [12]. Core losses cause energy losses in the core material due to eddy currents and hysteresis.

DCR Loss:

$$P_{dcr} = I_{rms}^2 \times R_{DC} \tag{2.2}$$

Core Loss:

$$P_{core} = K_f \times f_{sw} \times B^y \times V_e \tag{2.3}$$

Transistor Losses

Another source of loss is due to the transistor used in the DC/AC converter. In this thesis, the converter is implemented by a switch mode power amplifier. The main contributing losses are caused by the following transistor parameters: on-resistance, gate capacitor, and output capacitance. The losses from the transistor can be categorized into conduction and switching losses.

Conduction losses are caused by current flowing through the intrinsic resistance of the transistor when the transistor is turned on. The higher the on-resistance of the device, the more power dissipation there is every time the transistor turns on. Conduction losses also dominant more at higher power applications because the current through the transistor can get quite large. Switching losses such at the $P_{gateloss}$(input capacitance loss) and $P_{C_{oss}}$(output capacitance loss) are caused by the parasitic capacitances of the transistor getting charged up during turn off and discharged through the transistor during turn on. Switching losses are directly proportional to the switching frequency and how large the parasitic capacitors and gate charges are. If the switching frequency is increased, then more often the parasitic capacitors are charged and discharged. If

(a) Parasitic Capacitances   (b) Transistor Capacitances Model
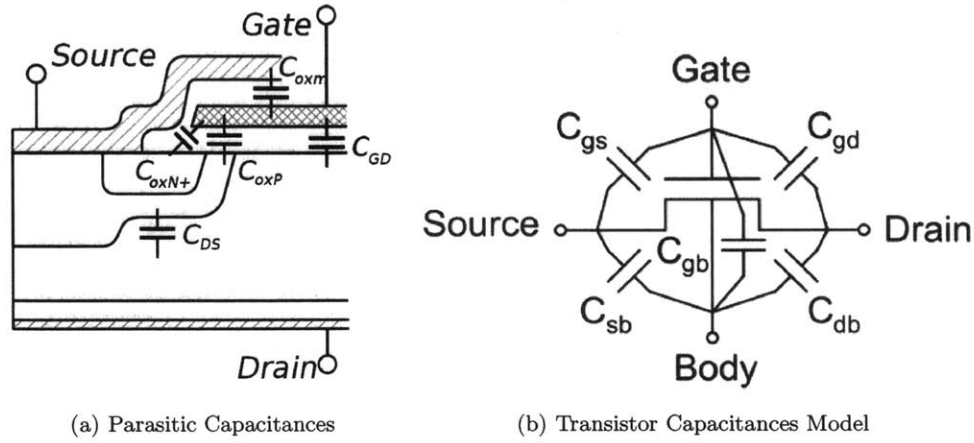
Figure 2.5: Capacitances of Transistor [29]

the parasitic capacitance values are higher, the more charge is wasted, and thus more wasted power. The main transistor losses follow these relationships:

$$C_{iss} = C_{GS} + C_{GD} \tag{2.4}$$

$$C_{oss} = C_{GD} + C_{DS} \tag{2.5}$$

$$P_{conduction} = I^2 \times R_{ds,on} \tag{2.6}$$

$$P_{gateloss} = Q_G \times V_{in} \times f_{sw} \tag{2.7}$$

$$P_{C_{oss}} = C_{oss} V^2 f_{sw} \tag{2.8}$$

■ 2.4.2 Receiver Side Losses

Coil Losses

The receiver side also has a secondary coil that contributes a significant amount of ACR loss. The same relationships hold as those on the primary coil.

Diode Losses

On the receiver side of the charger, diodes that can be used when implementing the rectifier are another source of loss. Though certain rectifier topologies are more efficient than others, diodes also have parasitics that are not negligible. In converters, diodes are either on or off throughout the cycle. When the diode is turned on, there is current flowing through the device and a forward voltage drop across the diode. Conduction losses for diodes also dependent on the current through the diode. $P_{conduction}$ losses can be minimized by using Schottky diodes which tend to have lower forward voltage drops. There is a trade off between how much reverse voltage the diode can block and the forward drop of the diode. To minimize the power dissipation, diodes should be chosen with the minimum necessary reverse voltage to reduce the forward voltage drop.

$$P_{conduction} = I_{out} \times V_{fwd} \tag{2.9}$$

An additional loss occurs when the diode transitions states from forward to reverse biased. The excess minority carriers in the pn junction need to be removed before the diode can turn off, but this cannot happen instantaneously as demonstrated in Figure 2.6a. The time it takes to remove the excess minority carriers is referred to as the reverse recovery time, t_{rr}. During the t_{rr} in Figure 2.6b, the voltage across the diode is nonzero because it is unable to turn off. Thus, there is significant reverse recovery current needed to move the excess minority carriers. With a nonzero voltage current product across the diode, there is significant power dissipation during the reverse recovery period.

■ 2.5 Efficiency

Understanding the sources of losses and their dependencies are the key to estimating how much power dissipation there is in the overall system. The efficiency of the overall system is characterized by the following:

$$\eta_{system} = \frac{PowerDelivered}{PowerConsumed} = \frac{P_{out}}{P_{in} + P_{drive}} \tag{2.10}$$

where,

$$TotalPowerLoss = P_{in} - P_{out} \tag{2.11}$$

(a) Reverse Recovery Origin   (b) Diode Current and Voltage Waveforms
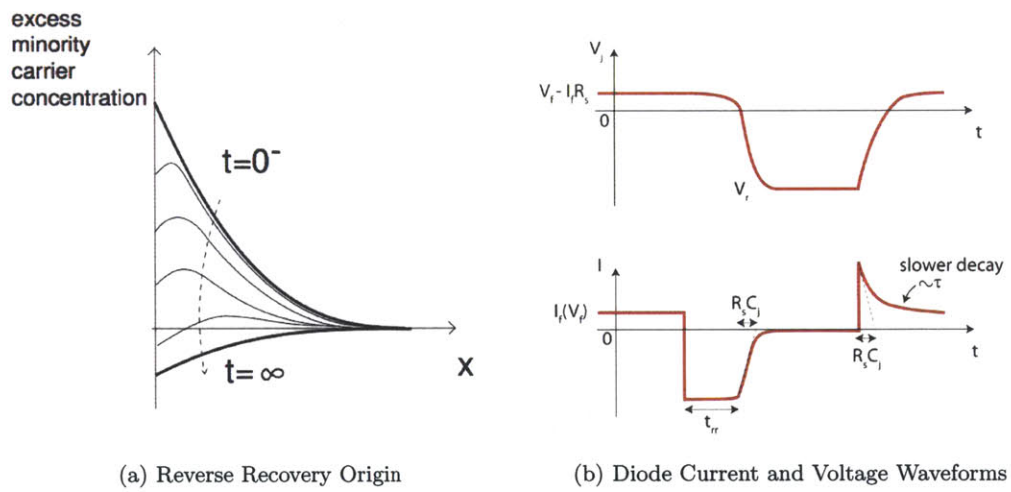
Figure 2.6: Reverse Recovery Loss [8]

Chapter 3

Coil Design

The first design choice to make is the operating frequency of the wireless charging system. Then, each component is carefully selected to be optimal at the desired frequency. The first components designed were the primary and secondary coils in the inductive resonant system.

■ 3.1 ISM Bands

Currently, the industrial, scientific and medical (ISM) radio bands are frequencies reserved for the use of radio frequency energy for industrial, scientific and medical purposes [5]. The powerful emissions of systems such as wireless charging can create electromagnetic interference and disrupt radio communication using the same frequency. Thus, there are limitations of certain band frequencies in which the wireless chargers can operate.

In this thesis, switching the circuit at 6.78MHz was a good starting point. 6.78MHz is the lowest ISM band and also provides reasonable converter size and efficiency. Higher frequencies such as 13.56MHz are explored further in Chapter 5.

■ 3.2 Self Resonance Frequency

Since the inductor coils only act inductive up to the self resonance frequency of the coil, it is best to operate the inductor a couple of octaves lower than the self resonance of the coil. After the self resonance frequency, the inductor starts to act like a capacitor and generates electric fields instead.

The circuit in this thesis is switching at the lowest ISM band, 6.78MHz. Thus, the self resonance frequency of the capacitors and inductors in the system need to at least 4-5x higher than 6.78MHz. Since off-the-shelf inductors did not provide high enough

self resonance frequencies, inductor coils were designed specifically for the system in this thesis. All inductor coils implemented were 2-D spirals flat on a PCB board.

■ 3.3 Size Constraints

■ 3.3.1 Secondary Coil

Since the target application in this thesis is smartphones, the entire receiver side should be within the dimensions of a cellphone. Generally, cellphones are between 2 to 3 inches wide and 4 to 6 inches tall. To have some buffer, the receiver coil show be smaller than 2 inches (50mm) in diameter.

■ 3.3.2 Primary Coil

This primary coil size is dependent on the size of the receiver coil. If the primary coil was the same size of the receiver coil, the two coils would need to be perfectly aligned to allow to efficient power transfer. To allow for a loosely coupled system where alignment between the primary and secondary coil has more flexibility and still maintain decent power transfer, the primary coil must be bigger. However the primary coil should not be bigger than necessary, otherwise the efficiency will suffer. Thus, the transmitter coil was designed to be about twice the diameter of the receiver coil (4 inches=100mm).

■ 3.4 Quality Factor

For the system to have high efficiency, it is essential for all components to have minimal losses. One of the main losses in inductive resonant chargers is the intrinsic resistance of the primary coil and secondary coil. High quality factor (Q) coils are necessary for efficient power transfer if there is flexibility in distance and misalignment between coils. The quality factor associated with the inductor coil gives a measure of how much series intrinsic resistance R is associated with the inductance L when operating at a fixed frequency f. Q is be calculated by:

$$Q = \frac{\omega L}{R} \tag{3.1}$$
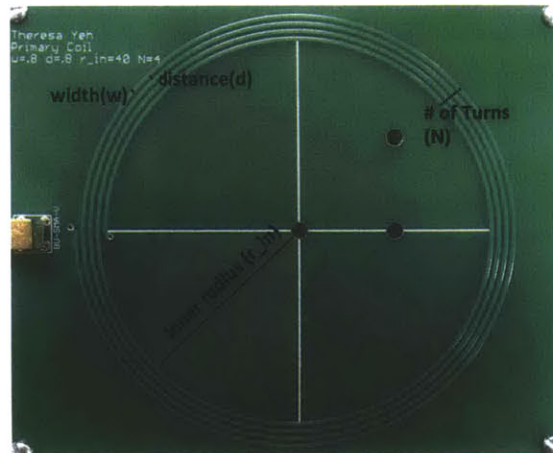
Figure 3.1: Coil Design Parameters

■ 3.5 Designing Optimal Coil

In summary, the primary and secondary coils need to stay within the size constraints
while maximizing the inductance and minimizing the intrinsic resistance (high Q). At
the same time, the PCB coil also needs a high self resonance frequency (at least 4-5x
the operating frequency). The parameters used to design the PCB coil are listed. The
primary coil implemented is shown in Figure 3.1.

    1) width: width of each trace

    2) distance: spacing between each trace

    3) inner radius: radius of the coil between traces start

    4) number of turn: number of full turns for entire coil

There are tradeoffs between each of the parameters to consider. Although increas-
ing the width of the traces lowers the intrinsic resistance, but the inductance value also
gets lowered. The inductance is proportional to N^2 and intrinsic R is proportional to
N. Thus, Q is proportional to N. Unfortunately, increasing N not only increases the
inductance but also the capacitance between the traces. If the capacitance becomes
significant, the self resonance frequency of the coil lowers. This runs the risk that
the inductive coil starts to act capacitive instead which can create electric field radia-
tion that affects the human tissue. The parameters of the primary and secondary coil
implemented are summarized in Table 3.1 and Table 3.2.

Table 3.1: Simulated vs. Actual Primary Coil Design Results at 6.78MHz

	TX #1	TX #2	TX #3
Width(mm)	1.5	0.8	0.8
Height(mm)	0.036	0.036	0.036
Spacing(mm)	1	0.8	4.2
Inner Radius(mm)	36	40	16
# of Turns	4	4	6
Inductance Real/Simulated (μF)	2.9/2.4	3.6/2.9	3.92/2.5
Resistance Real/Simulated(Ω)	1.7/0.4	2.5/0.8	4/0.8
Quality Factor Real/Simulated (Q)	105/255	92/155	60/133

Table 3.2: Simulated vs. Actual Primary Coil Design Results at 6.78MHz

	RX #1
Width(mm)	1
Height(mm)	0.036
Spacing(mm)	1
Inner Radius(mm)	10
# of Turns	4
Inductance Real/Simulated (μF)	0.79/0.6
Resistance Real/Simulated(Ω)	0.3/0.2
Quality Factor Real/Simulated (Q)	110/130

■ 3.5.1 Simulation vs. Actual Primary Coils

PCB coils were simulated in FastHenry simulations based on multi-pole accelerated algorithms [14]. PCB coils were built and the results of simulations versus actual measurements are also found in Table 3.1 and Table 3.2. The coil simulations had similar trends that were observed in the actual case, but there were differences in the absolute values. The larger the area of the coil, the more the discrepancy between the simulated and actual values. One hypothesis to explain this difference is that FastHenry simulations may not capture all the magnetic field generated leading to inaccurate results. More detailed explanations of the differences are explored in Chapter 5. The smith chart on the network analyzer is used to get an estimate of the inductance,

(a) caption 1

(b) caption 2
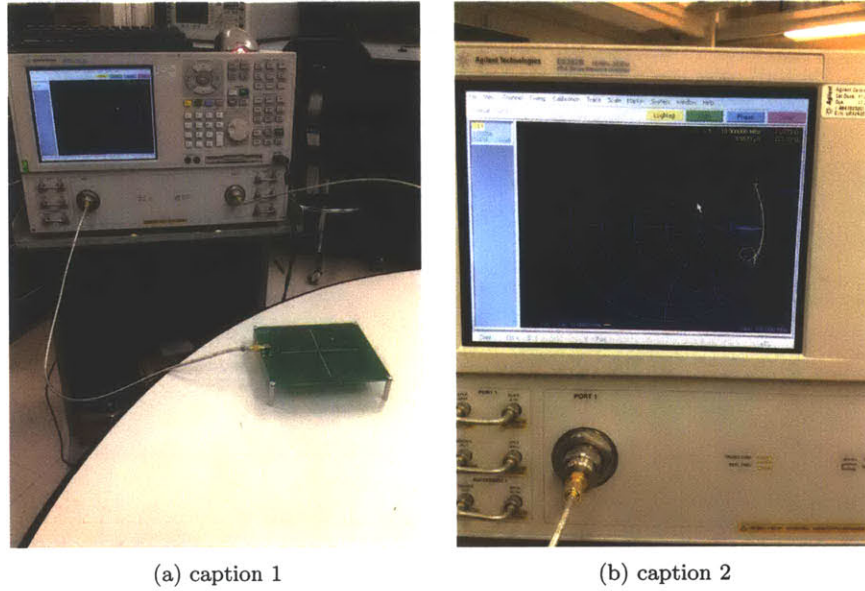
Figure 3.2: (a) Setup for measuring Primary Coil Parameters. (b) Actual Inductance and intrinsic resistance of Primary Coil using Smith Plot on Network Analyzer.

intrinsic resistance, and Q of each PCB coil. The setup for measurements are shown in Figure 3.2.

■ 3.6 Finding $Q_{L,opt}$

$$Q_{L,opt} = \frac{1}{k}\sqrt{\frac{Q_2}{Q_1}} \tag{3.2}$$

One of the key parameters of the wireless charging system can be calculated once the coil quality factors and coupling coefficient of interest are set. Using Equation 3.2 and Figure 3.3, the optimal load quality factor (Q_L) can be found for different coupling coefficients [23]. The maximum efficiency between the TX and RX coils (link efficiency) occurs when $Q_L = Q_{L,opt}$ for a specific coupling coefficient [2]. The higher the link efficiency, the less losses between the coils, and the higher the overall end-to-end efficiency. Methods to design the system to achieve $Q_{L,opt}$ is discussed in Chapter 4. Since users usually place their cellphones directly on the charging pad, the distance between the primary and secondary coil should be minimal. If k=.1 is set as the
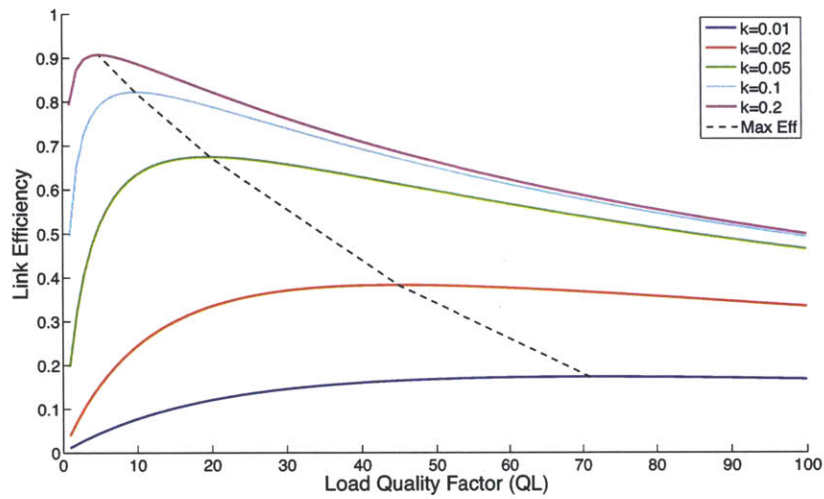
Figure 3.3: Finding optimal Q_L for different k ($Q1=Q2=100$)

coupling coefficient and both coils are designed to have $Q_1=Q_2=100$, then the best efficiency would be obtained when $Q_{L,opt}=10$. With the coil quality factors and $Q_{L,opt}$ set, the remaining components in the system can be calculated.

Chapter 4

Transmitter and Receiver Architecture

■ 4.1 Transmitter Architecture

■ 4.2 Building Blocks

The core element on the transmitter side of a wireless charging system is the power amplifier which is composed of a DC/AC converter with LC tank like in Figure 4.1. The inductor in the tank is the primary coil and the capacitor is added for resonance. Additional circuitry is necessary to provide the amplifier with the proper input drive. The main design choices made on the TX side were the operating frequency, type of DC/RF converter, and optimal components.

■ 4.2.1 Biasing the Power Amplifier

The DC/RF power amplifier on the transmitter side converts the supplied DC voltage into a high-frequency sinusoidal AC waveform which generates a magnetic field in the primary coil. From the wall AC mains, a rectifier and a step down converter can be applied to create the DC supply voltage needed for the power amplifier. The voltage
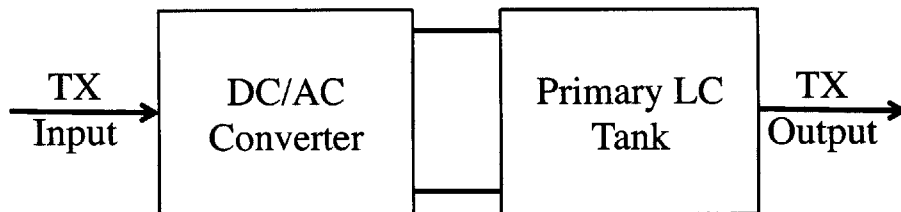
Figure 4.1: General Building Blocks of Transmitter System

supplied depends on the amount of power desired at the output and can be adjusted according to each specific application requirements. For the scope of this thesis, a DC supply will be connected to the power amplifier stage instead of implementing a rectifier from the wall voltage. This simplification is made because the main focus on this thesis is on the transistor losses in the power amplifier stage.

■ 4.3 RF Power Amplifiers

Because the DC/AC power amplifier (PA) consumes a significant amount of power, the losses of the PA become critical parameters in optimizing the system. Though every power amplifier is designed to operate slightly different, the quality of each power amplifier can be characterized by the following parameters: gain, efficiency, and linearity. Since the target application is for transferring power, efficiency is very important. Table 4.1 summarizes the theoretical maximum efficiencies for the various RF Power Amplifiers explored [19].

Table 4.1: Power Amplifier Efficiency Comparison

Type of PA	Theoretical Efficiency
ClassA	50%
ClassB	78%
ClassC	78% to 100%
ClassD	100%
ClassE	100%

In order to understand why the Class E amplifier was the design choice chosen, the basic advantages and disadvantages of each power amplifier class is briefly discussed.

■ 4.3.1 Conduction Mode Power Amplifiers: Class A, Class B, Class C

The first three types of RF power amplifiers shown in Figure 4.2 operate in conduction mode. The input and output of these amplifiers are all sinusoidal. Each class is distinguished by their biasing conditions, which leads to differences in the conduction angle. The conduction angle is the proportion of each input cycle where the transistor is passing current which closely relates to the efficiency of the amplifier. Class A, B, and C can all be understood by studying the model in Figure 4.2 and waveforms in Figure
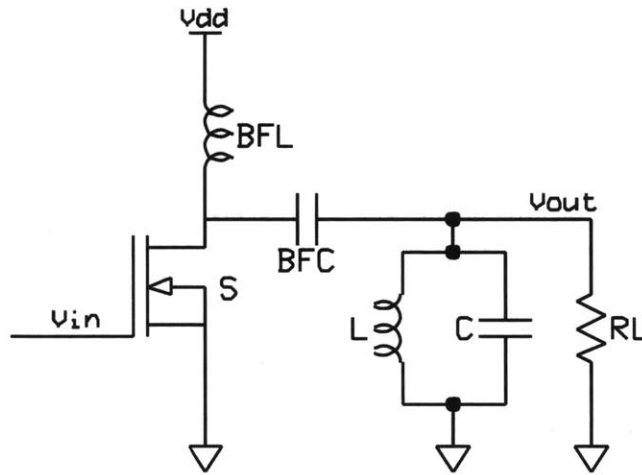
Figure 4.2: General Conduction Power Amplifier Model

(a) V_{GS} & I_D for Class A   (b) V_{GS} & I_D for Class B   (c) V_{GS} & I_D for Class C
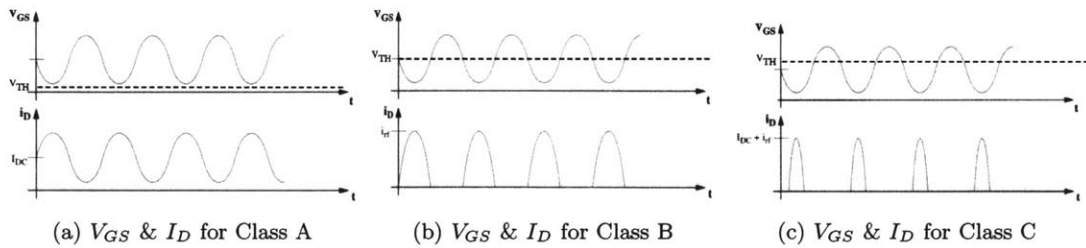
Figure 4.3: Conduction Mode Power Amplifiers

4.3. In the general model, R_L is the load where power is delivered. The large inductor, BFL, feeds constant DC current to the drain of transistor. The large capacitor, BFC, is used to prevent DC dissipation to the load. The high Q parallel LC tank is used to filter out the high frequencies to provide a sinusoid output even if fed nonsinusoidal currents. Specific operations of Class A, B, C are discussed further in T. Lee's book, H. Wai's paper, and the appendix [19] [27]. As shown in Table 4.1, conduction mode power amplifiers tend to have lower efficiencies. 100% efficiency in theory can only be attained at zero conduction angle and zero P_{out}.
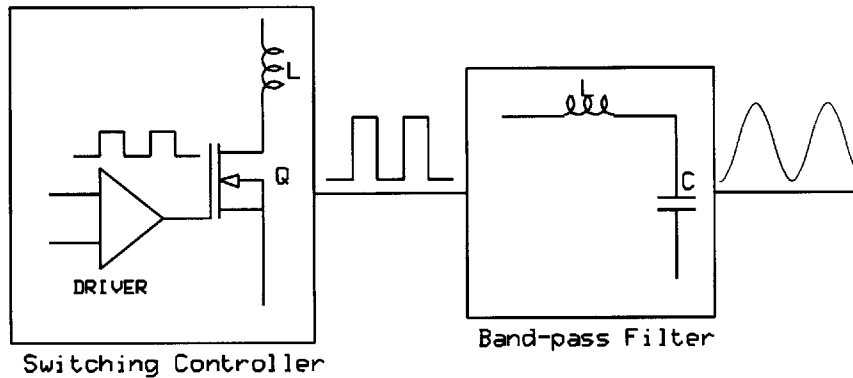
Figure 4.4: Switch Mode Amplifiers

■ 4.3.2 Switch Mode Power Amplifiers: Class D and Class E

Another approach to obtain higher efficiences is to operate the transistor as a switch instead. The basic operation and building blocks of switch mode power amplifiers are shown in Figure 4.4. The switching controller stage converts a DC supply into a square wave by turning on and off the transistor. Then, the square wave to fed through a band-pass filter to create a sinusoidal waveform. Though switch mode power amplifiers are more complex, there is potential for much higher efficiency. Switching amplifiers have higher efficiency because the transistor operates as binary switch that is either fully on or off, so that the product of the voltage and current waveforms are always zero. This is also under the assumption that no time is spent transitioning between on and off states. The improvement in efficiency comes at the cost of linearity. However, efficiency is much more important in a power transfer application.

The switching controller stage of the Class D amplifier is typically implemented by a stacked NMOS and PMOS. The input drives them complementary so that one transistor is always on and the other is off to provide a square wave output with variable duty ratio. Class D can also be implemented with full NMOS but the gate drive of upper transistor is complicated. To output a sinusoidal waveform, a second order band pass filter is cascaded with the first stage. Since the band-pass filter is composed of only inductors and capacitors, there is no power dissipation only energy storage in the filtering elements. Thus, Class D PA's can reach 100% efficiency in theory.

However in reality, there are nonidealties to consider. In Class D amplifiers, there is potential shoot through issues when stacking NMOS and PMOS with no transition time. For any amplifier, there are also parasitics in components which lead to the losses, reducing the actual converter efficiency. However, switching amplifiers can still provide the high efficiency by choosing components with low ESR and high Q. The goal of this thesis was to incorporate GaNFETs into the power amplifier to improve efficiency. Since Class D amplifiers either require an NMOS and PMOS or complex controller, Class D was not the best option because GaNFETs do not have a PMOS equivalent in market currently.

Fortunately, Class E amplifiers have the same efficiency benefits as Class D amplifiers but without this limitation. Figure 4.5 shows an ideal class E amplifier which consists of a switch S, an RF Choke (RFC), a tuned LC network formed by L_{TX} and C_{TX}, a load resistor R_L, and a capacitor $C1$ used to absorb the output capacitance of the switch. Class E amplifiers only need a NMOS switch. Thus, we can compare the efficiency of two systems with different switch implementations: one with NMOS and one with GaNFET. Another difference is that Class E amplifiers have an additional shunt capacitor to help achieve zero-voltage turn on. The operation of the Class E amplifier will be discussed in more detail in the next section. The main disadvantage of Class E amplifiers is that the peak drain voltage stress can reach up to $3.6V_{dd}$ [1]. This can be problematic if the transistor does not have high enough breakdown voltage. In this thesis, a MOSFET and a GaNFET with 200V breakdown voltage and 3A maximum DC current were implemented.

■ 4.3.3 Operation of Class E Amplifier

The basic operation of the Class E amplifier is the following [25] [24].

1) The transistor switch S is ON in half of the cycle and OFF in the other half.

2) When switch S is ON, the voltage across S is zero. When switch S is OFF, the current through the switch is zero.

3) The capacitance $C1$ absorbs the parasitic output capacitance of the transistor provided that $C1 > C_{oss}$.

4)The LC tank formed by L_{TX} & C_{TX} is tuned to resonant at approximately the fundamental frequency of input signal and passes a sinusoidal AC current into the load R_L.

5)There is zero voltage and zero slope switch turn-on across the switch due to the
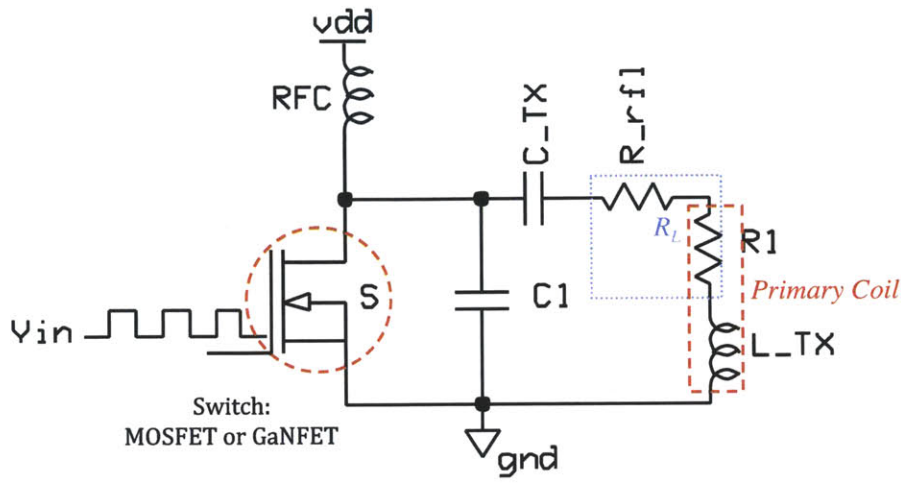
Figure 4.5: Class E Amplifier
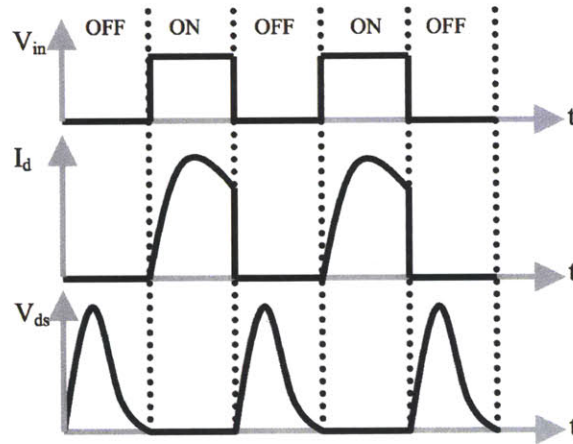
Figure 4.6: Ideal Class E waveforms [27]

addition of $C1$. $C1$ is discharged before S turns on every cycle.

■ 4.3.4 Optimal Waveforms

Ideal waveforms for a Class E power amplifier are shown in Figure 4.6. V_{in} is a square wave because the transistor is operated as a switch which is completely on or off. When the transistor is on, V_{ds} is zero and I_d is nonzero. When transistor is off, no current

flows and V_{ds} is nonzero. Ideally, the product of I_d and V_{ds} is always zero. The shunt capacitor is used to ensure that the V_{ds} returns to zero before the switch is turned on again [22].

Zero Voltage Switching(ZVS)

In ideal Class E amplifiers, ZVS occurs when there is zero voltage and zero slope during switch turn-on [13]. Adjustments in L_{TX}, C_{TX}, and C_1, all effect the switching waveforms of the PA. The goal is to allow $C1$ to discharge completely so the voltage across the transistor is zero before the switch turns on. If the voltage reaches zero before or after the switch turns on, the efficiency of the PA suffers.

If the voltage is still positive right before switch turn-on, the switch will suddenly bring the voltage down to zero by providing a low resistance path directly to ground. The intrinsic capacitor is discharged, which potentially can create a surge of current that destroys the transistor and wastes power. When the voltage hits zero and becomes negative before the switch turn-on, the switch body diode starts to conduct. Since the diode has forward voltage drop, this dissipates power as well.

ZVS is important for the Class E amplifier to obtain the optimal efficiency. However, the waveforms change depending on the system conditions such as distance and alignment. Though not implemented in this thesis, a control loop that automatically adjusts the components can be used to maintain ZVS and regulating power delivered [13].

■ 4.3.5 Calculations for Class E Amplifier Design

When designing the Class E amplifier, a couple design choices were made as a starting point. Component adjustments were made during implementation of actual system to optimize power transfer and efficiency.

The switching frequency of the Class E amplifier was set to the lowest ISM band (6.78MHz) because it provides the decent efficiency at a reasonable physical size. Coil 2 from Table 3.1 was chosen because it had a reasonably high inductance with minimal parasitic resistance and a Q_2 close to 100. With $Q_1=Q2=100$ and $Q_{L,opt}=10$, the loaded quality factors, Q'_1 and Q'_2 can also be determined for a fixed k. As mentioned earlier, the most realistic k was 0.1 for the implemented charging systems.

$$Q'_2 = \frac{\omega L_{RX}}{R_2 + R_L} = \frac{Q_2 \times Q_L}{Q_2 + Q_L} \tag{4.1}$$

$$Q_1' = \frac{\omega L_{TX}}{R_1 + R_{rfl}} = \frac{Q_1}{1 + k^2 Q_1 Q_2'} \tag{4.2}$$

With the f_{sw}, Q_1', and R_1 values known, the remaining parameters (R_{rfl}, C_1, C_{TX}, and P_o) of the Class E amplifier can be determined using the remaining equations [19]:

$$R_{loaded} = R_1 + R_{rfl} = \frac{\omega \times L_{TX}}{Q_1'} \tag{4.3}$$

$$C_1 = \frac{1}{\omega(5.447 \times R_{loaded})} - C_{oss} \tag{4.4}$$

$$C_{TX} = C_1(\frac{5.447}{Q_1'})(1 + \frac{1.42}{Q_1'} - 2.08) \tag{4.5}$$

$$P_o = \frac{V_{dd}^2}{R_{loaded}} \times .577 \tag{4.6}$$

The R_{loaded} is composed of R_1 and R_{rfl}. The R_1 is the intrinsic resistance of the primary coil and R_{rfl} is the optimal reflected impedance of the receiver circuitry. Implementation of the receiver circuitry to provide the necessary impedance for optimal efficiency is discussed next. $C1$ is the shunt capacitor that provides zero voltage turn on for optimal efficiency and absorbs the output capacitance of the transistor. C_{TX} is the capacitor in the primary LC tank. P_{out} is the total power coming out of the transmitter side. The V_{dd} value can be adjusted for each application that has a different desired output power. In this thesis, for desired deliverable power in the 3W-5W range, V_{dd} in the 10V-15V were necessary.

The hand calculation results of Class E amplifier components are shown in Table 4.2. These values set a good starting point for simulations. Actual components on the transmitter board were tweaked to compensate for variations in components to give the optimal efficiency. Since for every coupling coefficient, there is a set of different optimal parameters, parameters were found to give the optimal results at one fixed k (k=.1) and reasonable efficiencies for other k. To keep comparisons fair, measurements of the MOSFET and GaNFET systems were taken for the same coupling coefficient and same power delivered.

Table 4.2: Hand Calculations for Class E Design

f_{sw}	$Q_1=Q_2$	$Q_{L,opt}$	Q_1'	L_{TX}	R_{loaded}	C_1+C_{oss}	C_{TX}	P_o
6.78MHz	100	10	10	$3.6\mu F$	15Ω	300pF	180pF	15W
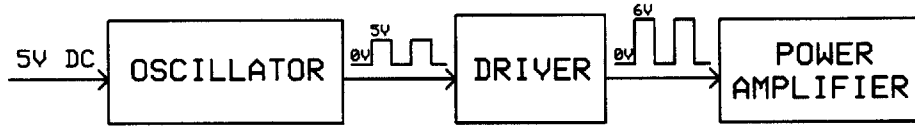
Figure 4.7: System Diagram for Driving the Power Amplifier

■ 4.4 Drivers

Now that the Class E amplifier components have been determined, the next step is driving the circuitry. A square wave drives the gate of the transistor so that it can operate as a switch: either fully on or fully off. Since the transistor is operating at high frequencies and high currents, the driver needs to be able to sink and source enough current to the circuitry. The LM5114B was used to drive both the MOSFET and GaNFET because of its strong ability to sink and source current. In addition, the driver's fast switching speed and propagation delays allow for high frequency operations. The driver was also designed to minimized switch node ringing from parasitics. The square wave is at 0V when the switch is fully off and V_{GS} when fully on. The optimal V_{GS} to turn on each switch was chosen to minimize overall transistor losses.

In order to use the LM5114B driver, a TTL input is necessary to provide a incoming square wave of 0 to 5 volts. An adjustable RC oscillator, LTC6900, was chosen. The resistors associated with the oscillator set the square wave desired 6.78MHz that drove the remaining circuitry.

■ 4.5 Receiver Architecture

■ 4.6 Building Blocks

Once the changing magnetic field is generated on the primary side, the secondary coil picks up a portion of the field and induces a voltage. The secondary LC tank should be tuned approximately to the same resonant frequency as the primary LC tank for
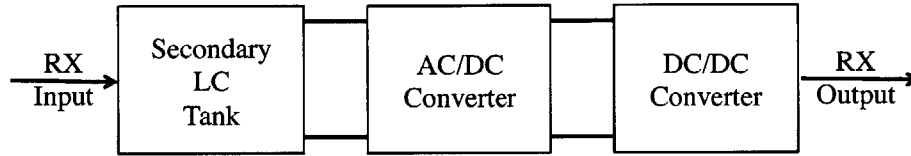
Figure 4.8: General Building Blocks of Receiver System

optimal power transfer. Then, a rectifier converts the AC current into a DC current and voltage. Finally, a DC/DC voltage regulator is used to provide the proper voltage and current delivered to the load. For a cellphone application, the DC voltage into the load is set for 5V with current up to 1A. The voltage regulator sets the output voltage to 5V. The V_{dd} which adjusts the output power limits the current delivered to the load. The overall receiver system diagram is shown in Figure 4.8. The receiver inductance L_{RX} and intrinsic resistance $R2$ are set by the receiver coil. With L_{RX} fixed, C_{RX} is adjusted for the desired resonant frequency.

■ 4.7 Series RLC Tank vs. Parallel RLC Tank

There are two methods to implement the secondary tank: series or parallel. The primary and secondary coil can be thought of as a transformer. Since the voltage across the primary coil is large and number of turns are the same, the voltage across the secondary coil must also be large. However, different arrangements of the inductor, capacitor, and resistor in the tank will alter the output voltage, power delivered, and system efficiency.

Series and parallel tanks each have its advantages and disadvantages. The most fundamental case is the unloaded LC tank which will be discussed first.

Unloaded LC tank

In the unloaded case (without a resistor) shown in Figure 4.9, a general LC tank has high voltages across the inductor and capacitor at the resonant frequency. At the resonant frequency, the impedance of the capacitor and inductor also cancel. Thus, with high voltage and low impedance, large currents go through both the inductor and capacitor in the tank. However, since the inductor and capacitor voltages are out of phase, the sum of the voltage around the loop is relatively small.

Figure 4.9: LC tank
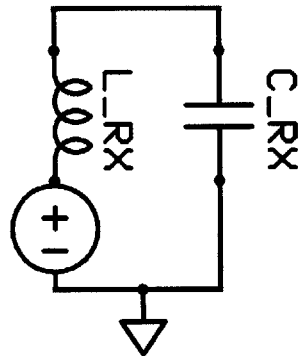
(a) series RLC tank   (b) parallel RLC tank
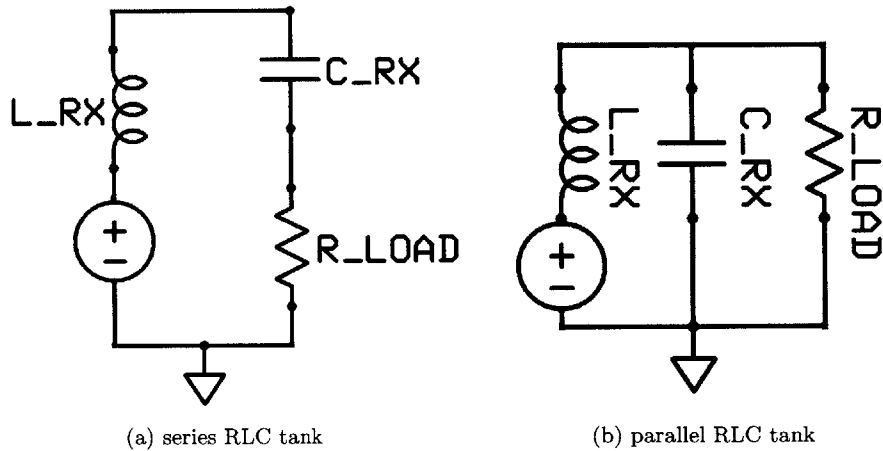
Figure 4.10: RLC tanks

Loaded LC tanks

Where the load resistor is placed determines whether it is a series or parallel RLC tank.

$$Power_{OUT} = \frac{V_{Load}^2}{R_{Load}} \tag{4.7}$$

In a series RLC case like Figure 4.10a, since there are large voltages across the inductor and capacitor, the voltage left across the resistor, V_{Load} is very small. The power out is set by the voltage across the resistor(V_{Load}) and the resistance (R_{Load}) in Equation 4.7. Cellphones typically can only handle a maximum of 5W. From Equation

4.7, in order for the $Power_{OUT}$ to be small, the R_{Load} also needs to be small since the V_{Load} is small. The main advantage of using series RLC tank is that the output voltage can be lower and close to the 5V that the cellphone wants. However, there are some other considerations. The R_{Load} is the impedance seen through the output resistor and the rectifier diodes in series. Thus, most of the resistance is dominated by the parasitics of the diodes in the rectifier, which decreases the efficiency of the system.

On the other hand, parallel RLC tanks such as Figure 4.10b behave in the opposite way. Since when the inductor, capacitor, and resistor are all in parallel, they all share the same high voltage. Using Equation 4.7, the R_{Load} must be large to get reasonable power out from the load. Though the advantage here is that the resistance of the diodes of the rectifier no longer dominant, but the output can be much great than the desired 5V. For a cellphone application, this means that an extremely high voltage must then be brought down to 5V. For the step-down converter, the duty ratio would need to be very small and there would be extremely high stresses on the components in the converter. For the same power desired, high stresses on the voltage regulator reduces both the DC/DC converter efficiency and the overall wireless system efficiency [20].

The differences between a series and parallel RLC tank are summarized in Table 4.3.

Table 4.3: Series versus Parallel RLC Tank

Type of RLC	Output Voltage
Series RLC	LOW
Parallel RLC	HIGH

Based on the simulations, the parallel RLC was producing output voltages that were much higher than the desired 5V. Thus, a series RLC tank was implemented even though the parasitics of the diodes in the rectifier became significant. To minimize the losses from diodes, schottky diodes that had the minimum necessary breakdown voltages were chosen. The receiver side block diagram implemented is shown in Figure 4.11. Specific types of diodes and rectifier topologies are discusses the next section.

■ 4.8 Half Bridge Rectifier vs. Full Bridge Rectifier

The two rectifier topologies that were explored in this thesis were the half bridge and full bridge rectifier. Because the focus of this thesis is the to show the difference in system
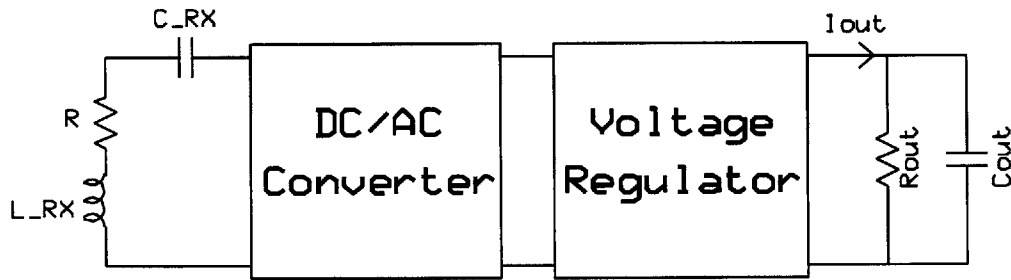
Figure 4.11: Receiver Side Block Diagram

efficiency when using MOSFET or GaNFET on the transmitter side, more complex rectifier topolgies that may provide better efficiency were not explored.

The half bridge rectifier shown in Figure 4.12a is the most simple. However, there are issues because of the capacitor in the LC tank in series with the rectifier. In periodic steady state, the current in a capacitor must be zero. However, since there is only one diode and half cycle of conduction, charge builds up on the capacitor and the voltage across the capacitor will eventually get to the point that the diode can no longer conduct and the rectifier stops functioning. This issue can be solved by adding a free wheeling diode so the current has a path for both parts of the cycle. However, since there's high voltages across the L_{RX}, the free-wheeling diode dissipates power during half the cycle.

Thus, the next option explored was the full bridge rectifier as shown in Figure 4.12b. In one half of the cycle, current flows through two diodes and the load resistor in series. In the other cycle, current flows through the other two diodes and the load resistor. Although there is now two diode drops instead of one diode drop every cycle, the efficiency is still higher because the the free wheeling diode discharges the high voltage inductor, dissipating even more power.

■ 4.9 Optimal Load

$$Q_{L,opt} = \frac{\omega L_{RX}}{R_{Load}} \qquad (4.8)$$

Now that the receiver building blocks and optimal $Q_{L,opt}$ have been determined, the last step was to determine the load resistance, R_{OUT}, that would give the highest end-to-end system efficiency. From Chapter 3, $Q_{L,opt}$ was found to be 10 and the receiver coil inductance, L_{RX}, was set to .79 μH at 6.78MHz. Finding R_{Load} first helps

(a) Half Bridge Rectifier   (b) Full Bridge Rectifier
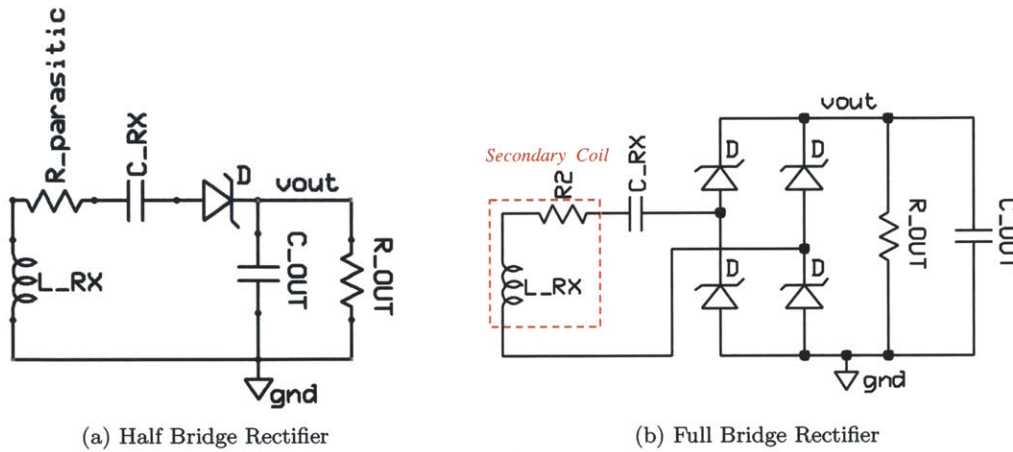
Figure 4.12: (a) Rectifier Topologies

with determining the optimal R_{OUT}. Using Equation 4.8, the optimal R_{Load} can be calculated for the system in Figure 4.13a. However, the full bridge rectifier needs to been incorporated into the system while maintaining the same impedance seen into the AC port. To maintain the same maximum efficiency, the impedance seen into the rectifier and R_{OUT} should be approximately equal to R_{Load} as Figure 4.13c. A simple way to determine to the optimal R_{OUT} from Figure 4.13c is the following:

1) Measure the voltage and current waveforms across R_{Load} in Figure 4.13a.

2) Set voltage across R_{Load} as the v_{ac} in Figure 4.13b.

3) Adjust R_{OUT} in Figure 4.13b until I_{AC} coming out of v_{ac} is same as I_{AC} across R_{Load} from Step 1.

4) Once the I_{AC} is the same, the impedance seen into AC port should be equivalent to R_{Load} as shown in Figure 4.13c.

To achieve the optimal efficiency for the overall system, the R_{OUT} should be the load at the output.

■ 4.10 Voltage Regulator for Charging Cellphones

Though a rectifier can provide a DC output to the load, an additional stage is necessary for voltage regulation for charging a cellphone. Depending on the variations between distances, offsets, and other factors, the output voltage can easily be affected. The rectifier only needs to provide a valid input voltage and then the voltage regulator will
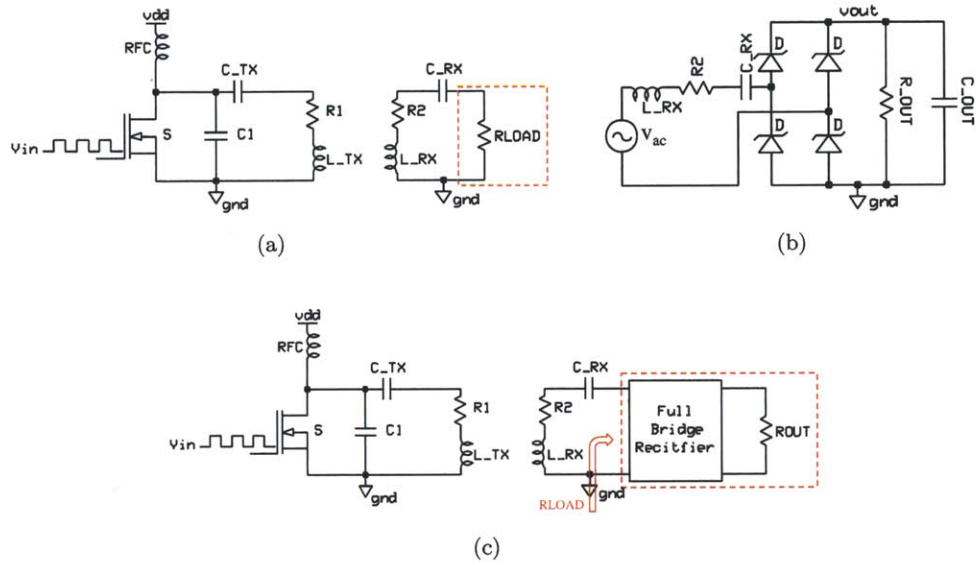
Figure 4.13: (a) Rectifier Load Optimization

produce the proper voltage output that the load needs. In this thesis, a boost converter was implemented to always output 5V if given an input voltage from the rectifier output in the 1.8V-6V range. A zener diode with a breakdown of 6V was also placed at the input of the boost in case the input voltage reached a value higher than 6V. In this situation, the input voltage will be clamped down to 6V, such that the boost regulator can still operate properly and output the desired 5V output to the cellphone.

Chapter 5

Results and Analysis

Wireless charging transmitter and receiver boards were designed and implemented as shown in Figure 5.1. The main difference between the two systems is the switch implementation on the transmitter board: Silicon MOSFET versus Gallium Nitride FET. For a fair comparison, the circuit topology, layout, and components were as consistent as possible. The capacitors, C_1 & C_{TX}, and voltages, V_{in} & V_{dd}, were adjusted to provide the optimal efficiency for each individual system. Efficiencies were compared when both systems provided the same $Power_{out}$. In addition to analyzing efficiency differences due to different transistors, other factors such as distance and alignment of boards were also explored.

■ 5.0.1 Test Setup Conditions

End-to-end system efficiency measurements were taken with the receiver board in Figure 5.1b, which includes the secondary tank, rectifier, and optimal R_{OUT}. Losses from the voltage regulator and driver circuitry were not included in the end-to-end efficiency measurements. The combined receiver board which also had a voltage regulator stage in Figure 5.1d was only used in demos and not during testing.

■ 5.0.2 Distance vs. Coupling Coefficient

As the distance between the primary and secondary coils increase, the coupling coefficient decreases. The coupling coefficient plays an important role in how efficient the wireless charging system is. The higher the coupling coefficient, the more flux that is generated from the primary coil is received or coupled onto the secondary coil. As shown in Figure 5.2, there is an inverse relationship between distance and coupling coefficient.

Since the systems were designed to allow for misalignment, the maximum coupling

(a) MOSFET TX Board   (b) RX Board Used for Testing

(c) GaNFET TX Board   (d) RX Board Used in Demos
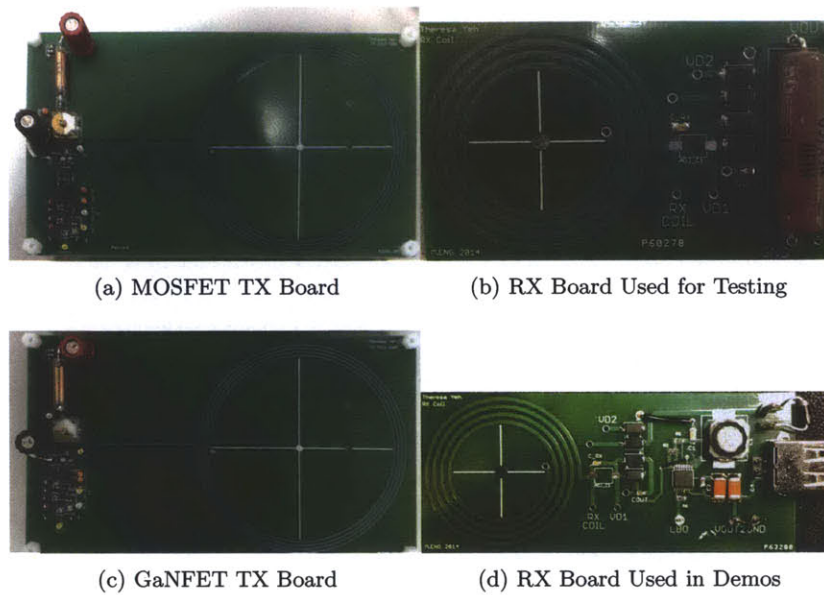
Figure 5.1: TX and RX Boards
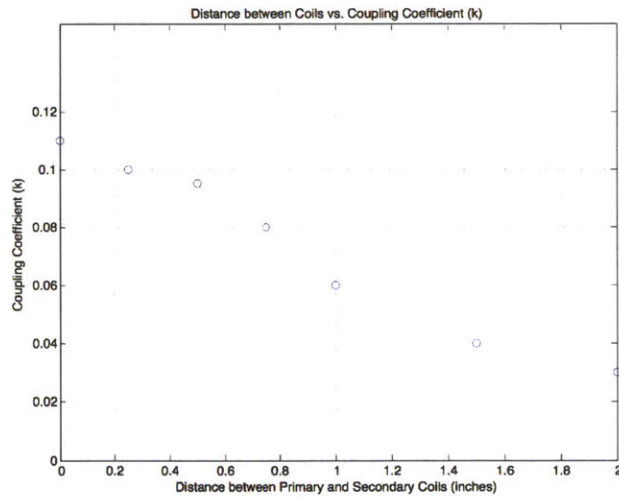
Figure 5.2: Distance between Primary and Secondary Coils vs. Coupling Coefficient

coefficient is k=.11 when the secondary coil is directly on top of the primary coil. When coils are at 2 inches apart, the k=.03. As the distance between the coils decrease, the coupling coefficient increases. However, the behavior is nonlinear. After certain

(a) center offset   (b) side offset   (c) diagonal offset
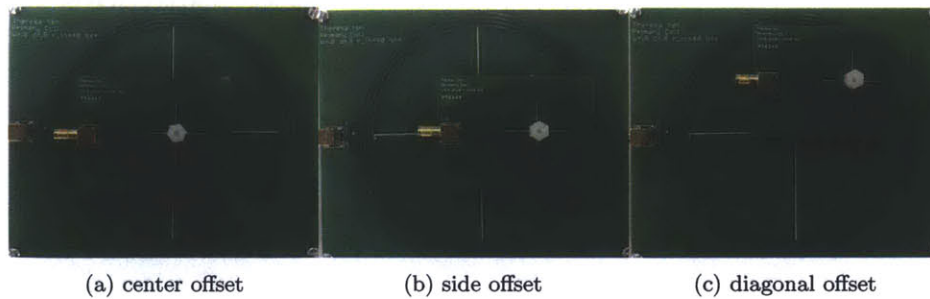
Figure 5.3: Offsets Between Primary and Secondary Coil

distances, the coupling coefficients do not change much. For example, the coupling coefficient difference between 0" and 1/2" is not that significant. However, difference between 1/2" and 1" are much more significant. Similarly, distances greater than 1.5" do not decrease the coupling coefficient much.

■ 5.0.3 Offset vs. Coupling Coefficient

The primary and secondary coil were placed in three different alignments as shown in Figure 5.3. Figure 5.3a shows when the coils are perfectly aligned. Figure 5.3b shows when they are slightly misaligned and Figure 5.3c shows even more misalignment. When measuring the coupling coefficient of all three offsets, the coupling coefficient remains the same. The design choice made was for the transmitter coil to be double the size for receiver coil to allow for misalignment. Thus, the receiver coil seems to be able to capture the same amount of magnetic flux as long as the receiver coil is placed somewhere within the primary coil area. However, if the primary coil size decreases in size, the effects of misalignment will reduce system efficiency more and more.

■ 5.0.4 Coupling Coefficient vs. Overall System Efficiency

Because the amount of magnetic flux the secondary coil captures is directly related to the coupling coefficient, the coupling coefficient directly impacts the overall system efficiency. The higher the coupling coefficient, the more flux is captured, and the loss from the coils is reduced. From Table 5.1, as the distances decreases, the efficiency of coils and overall system improve.

The same trend can been seen in both the MOSFET system and GaNFET system

because the coupling coefficient is only determined by the primary and secondary coils. Since the same coils were implemented for both systems, the coupling coefficient should be consistent.

End-to-End Efficiency Comparison between MOSFET and GaNFET system

Though the distance versus efficiency inverse relationship is consistent for both systems, the GaNFET system always provides a 5% efficiency gain over the MOSFET system over a range of distances. This is due to the lower parasitics of the GaNFET system since the remaining circuitry is consistent and optimized for the system.

Table 5.1: Coupling Coefficient vs. Overall System Efficiency Comparison

Distance (inches)	Coupling Coefficient (k)	Efficiency GaNFET System	Efficiency MOSFET System
1	.06	30%	25%
1/2	.095	45%	40%
1/4	.1	50%	45%

■ 5.0.5 Offset vs. End-to-End Efficiency

Because the primary coil is double the size of the secondary coil, the efficiency stays constant regardless of misalignment. If the receiver coil remains within the primary coil, the receiver coil can be placed anywhere and still capture similar amounts of magnetic flux that has been generated from the primary coil. This is consistent with how the offset does not change the measured coupling coefficient. Again, the same trends are seen in both the MOSFET system and GaNFET system because the coupling coefficient is coil dependent.

Table 5.2: Receiver Coil Offset vs. Overall System Efficiency (k=.1)

Position of Secondary Coil (k)	Efficiency(GaN)	Efficiency(MOS)
Center	50%	45%
Side	50%	45%
Diagonal	50%	45%

■ 5.0.6 Class E Waveforms for Different Distances

Power loss is directly proportional to the product of $I_{ds} \times V_{ds}$. In Figure 5.4c, when coils are closest at k=.1, ZVS is almost achieved, resulting in the best efficiency. This is because the I_{ds} and V_{ds} product is smallest, dissipating the least amount of power. As the distance increases, V_{ds} hits zero before the switch is turned on again. When V_{ds} hits zero too early, the reverse diode takes effect, clamps V_{ds} to -0.6V, resulting in a nonzero I_{ds} and V_{ds} product during this gap period. The gap and the power loss increases as the distance between the coils increase as shown in Figure 5.4. The timing of the waveforms were controlled manually in this thesis. In future work, it would be more effective to implement a control loop that achieves reliable and optimal timing automatically.

(a) 1" between Primary and Secondary Coil

(b) 1/2" between Primary and Secondary Coil

(c) 1/4" between Primary and Secondary Coil
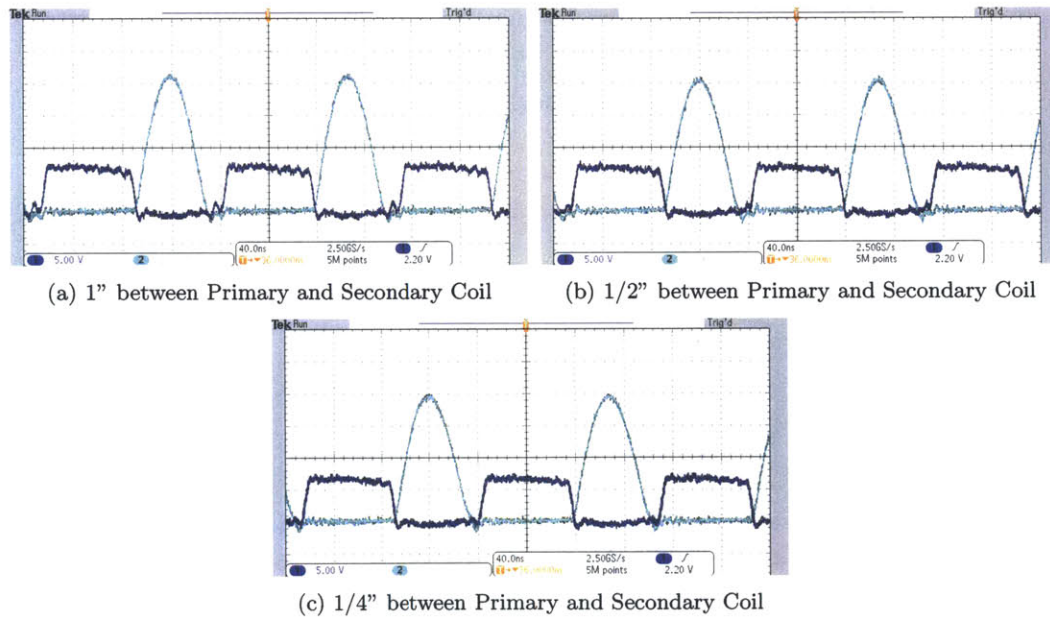
Figure 5.4: V_{in} and V_{ds} waveforms for Different Distances between Coils

■ 5.1 Analysis

The results section show the measurements taken on the implemented MOSFET and GaNFET systems. To better understand the differences, the losses in these systems are

analyzed further through simulations. The simulations were done on the end-to-end system, excluding losses from the voltage regulator and driving circuitry.

■ 5.1.1 Breakdown of Losses in Overall System

The breakdown of losses between the two end-to-end systems are compared in Figure 5.5. Component and voltage adjustments were made to optimize each individual system. The systems were compared under the same coupling coefficient (k=0.1) and same power out ($P_{out} = 4W$).

Since the parasitics (on-resistance and parasitic capacitances) of the MOSFET are significantly worse than those of the GaNFET, the absolute transistor losses in the MOSFET system are almost double of those in the GaNFET system. The other absolute losses are relatively similar between the two systems. From Figure 5.5, the transistor losses in MOSFET system accounts for 2% more of overall losses than the GaNFET system because the switch parasitics make more of an impact. However, with the other losses relatively the same, the overall efficiency was reduced by the additional transistor losses.

(a) $P_{in} = 6.67W, P_{out} = 4W, P_{loss} = 2.67W,$(b) $P_{in} = 6.83W, P_{out} = 4W, P_{loss} = 2.83W,$
$\eta_{simulated} = 63\%$ $\eta_{simulated} = 58\%$
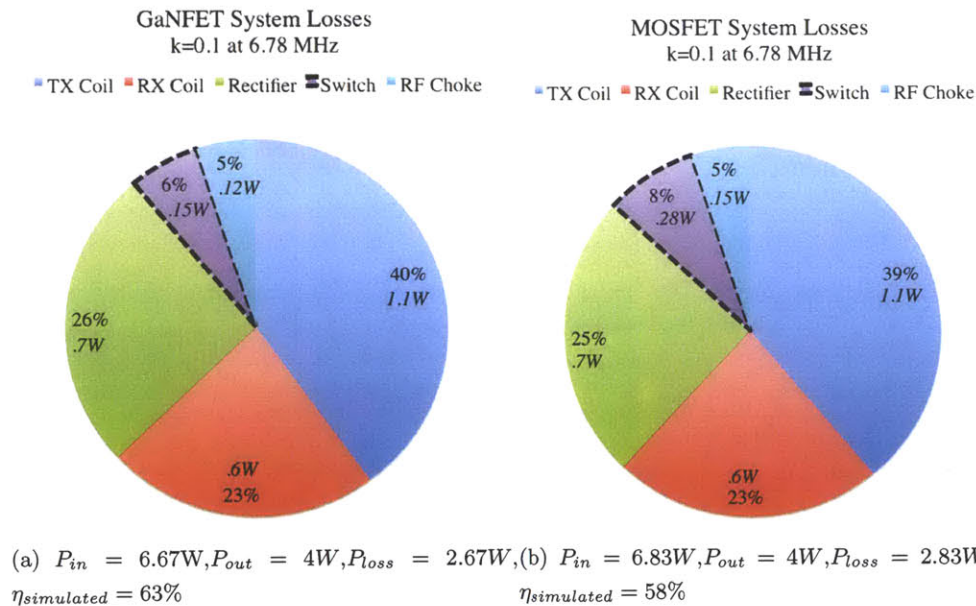
Figure 5.5: Comparison of Breakdown of Losses for GaNFET and MOSFET system

■ 5.1.2 Coupling Coefficient vs. Overall System Losses Breakdown

As the distance between the coils decrease, the coupling coefficient increases. Thus, the losses from the coils are reduced and less dominant. From Figure 5.6a, the coil loss is greater and accounts to 60% of the total power loss. However, if the distance is smaller, the coil losses decrease dramatically as seen in Figure 5.6b. Tightly coupled coils not only reduces the coil losses but also the total power loss. Thus, the coupling plays an important role in improving efficiency as well as in Table 5.3.
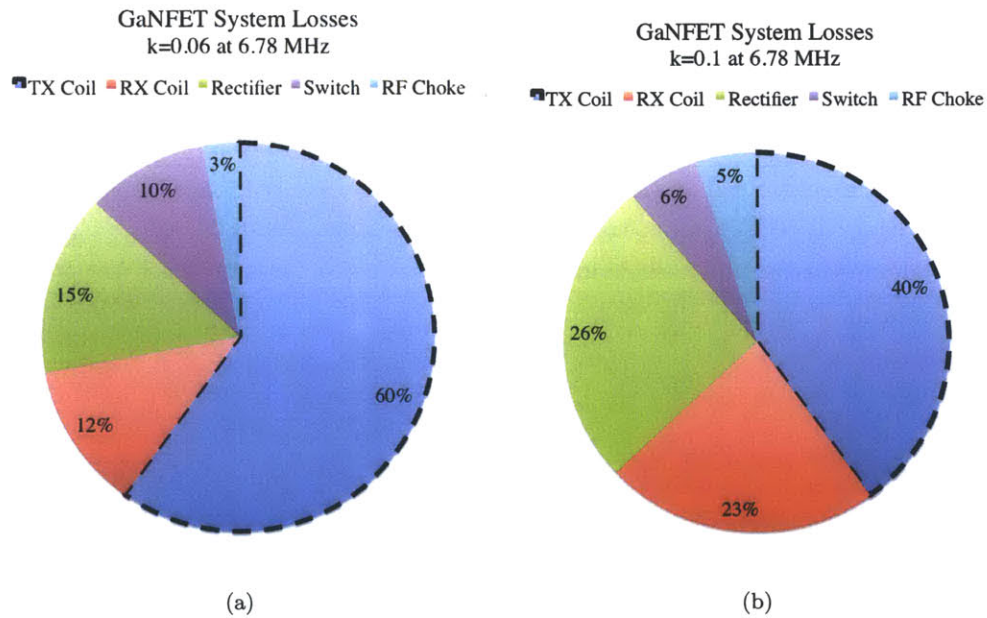
Figure 5.6: Comparison of Breakdown of Losses for GaNFET

Table 5.3: Coupling Coefficient vs. Overall GaNFET System Efficiency

	k=.06	k=.1
Vdd (V)	15	15
Power Loss Total (W)	4.2	2.6
Overall Efficiency Actual/Simulated(%)	30%/45%	50%/63%
Total Coil Loss (W)	2.5	1.1

■ 5.2 Breakdown of Losses on Transmitter Side

Breakdown of Losses on Transmitter Side: GaNFET system

Breakdown of Losses on Transmitter Side: MOSFET System

Source of Loss	k=0.06		k=.1		Source of Loss	k=0.06		k=.1	
RFC	5%		12%		RFC	5%		9%	
TX Coil	81%		78%		TX Coil	78%		77%	
Gate Drive	1%		2%		Gate Drive	5%		4%	
Conduction	12%	14%	8%	12%	Conduction	11%	16%	9%	14%
Output Capacitance	1%		2%		Output Capacitance	1%		1%	

(a)   (b)

Figure 5.7: Comparison of Breakdown of Losses for Transmitter Side

Since the differences between the systems are on the transmitter unit, the breakdown of losses are examined on the transmitter side. The Class E amplifier is composed of the following: RFC, TX Coil, transistor, and capacitors. As discussed in Chapter 2, each component contributes individual power loss due to parasitics. For the analysis, capacitor losses were negligible because the capacitors used were high Q low ESR ceramic capacitors.

As expected, the AC current running through the intrinsic resistance from the TX coil is the most dominating loss. The next significant loss is due to the transistor. The least significant loss is from the DC resistance and core of the inductor.

The overall transistor loss is composed of the gate drive loss ($P_{gateloss}$), conduction loss($P_{conduction}$), and output capacitance loss(P_{Coss}). Since the shunt capacitor in Class E amplifiers absorbs the output capacitance, the output capacitance loss is minimal. Because of the product of $Q_G \times R_{ds,on}$ for the MOSFET is around 15x more than that of the GaNFET, the parasitics cause much more power dissipation. Table 5.7 shows the breakdown of losses from simulations. At $f_{sw} = 6.78MHz$, the conduction loss is the main transistor loss because it takes up majority percentage of total transistor loss. Though the conduction loss is the dominant loss, the $P_{gateloss}$ is the main differentiator. At k=0.06, the GaNFET $P_{gateloss}$ only accounts for 1% of total transistor loss. However, in the MOSFET system, the $P_{gateloss}$ contributes 5%. At 6.78MHz, the biggest difference in the parasitics was the gate charge. As the switching frequency increases, the absolute switching losses due to the parasitic capacitors start charging and discharging more and can become much more significant, reducing the overall efficiency greatly.

Table 5.4: Simulated vs. Real Coil Parameters

Coil	Inductance (μH) (Simulated/Real)	Resistance(Ω) (Simulated/Real)	Diameter(inches) (Simulated/Real)
Primary	2.5/3.6	.8/2.5	4/4
Secondary	.6/.79	.2/.3	2/4

■ 5.3 Differences Between Simulated and Actual

Although simulated values were a good starting point, there were many differences between the simulated and actual measurements taken. The potential cause of these differences are explored further in this following section.

■ 5.3.1 System Efficiency

The transistors and the diodes were the only components with simulation models in LTSpice. All other components had their parameters estimated through the datasheet and inputted manually. Thus, these variations can lead to differences in simulated versus actual efficiencies.

During simulations, although the DC resistance of the RFC was accounted for, the core loss was not. Since the capacitors implemented are high Q, low ESR, losses were ignored in simulations. Because simulated coil inductances and resistances were very different from actual parameters, the TX and RX coils were built and measured separately. These measured values were the values put into simulations to decrease the inaccuracy. However, it is still very difficult to measure the coils with high accuracy on the Network Analyzer. All of these component variations could have contributed to the differences in simulated vs. actual system efficiencies.

■ 5.3.2 Coil Parameters: L, R

A comparison between simulated and actual coil parameters are in Table 5.4. The actual inductance value of coils are always larger than the simulated inductance in FastHenry. One possible explanation is that FastHenry does not capture the whole picture. FastHenry passes current through the coil in order to measure the magnetic field generated and the energy density of the magnetic field. From these measurements, it can deduce the inductance value. However, it is possible that the area taken into account does not fully capture all the magnetic field energy, which in turn reduces the
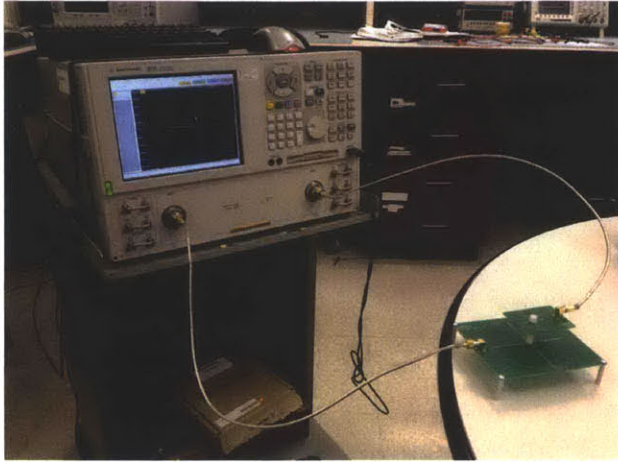
Figure 5.8: Setup for measuring coupling coefficient (k) between coils

inductance value.

■ 5.3.3 Coupling Coefficient

Table 5.5: Simulated vs. Actual Coupling Coefficients

Distance between Coils	Simulated k	Actual k
0"	.11	.11
1/4"	.11	.1
1/2"	.11	.095
3/4"	.11	0.8
1"	.11	0.6
1.5"	.08	0.4
2"	.08	0.3

The same hypothesis is used to explain why the coupling coefficient simulated are slightly different from the actual values. However, the coupling coefficient in simulations still give a good order of magnitude estimate. Actual measurements of the coupling coefficient were measured with the Network Analyzer as shown in Figure 5.8. The comparison between simulated and actual coupling coefficients are found in Table 5.5.

■ 5.4 Power Transfer Demos

Two applications of wireless power transfer are demonstrated in this thesis: charging a LED board and charging a cellphone.

■ 5.5 Charging LEDs

The LED Demo provides a visual representation of successful wireless power transfer from the primary to secondary unit. The LED Demo board is connected to the output of the receiver unit which includes the secondary LC tank, a full bridge rectifier, and a boost converter that produces the proper 5V and desired current to power the LED board. The V_{dd} on the transmitter side can be adjusted to meet the desired power out. For all the LEDs to shine at maximum brightness, then 5W (5V/1A) is necessary.

The "MIT" logo is made with 5 sets of 5 red LEDs in parallel. Each individual LED draws 20mA of current and has a 2.1V forward voltage drop. Because the desired output is 5V, these 5 parallel LEDs are in series with a 29 ohm resistor with a 2.9V drop and 100mA of current.

The star shape made from clear LEDs is 10 sets of 2 LEDs in parallel. Again, each of these sets are connected to a series resistor. In this case, 10 sets of 2 parallel led branches with 40 ohm resistor to set the 20mA through each LED.

The boost output regulator in this thesis is designed to output a fixed 5V. Additional circuitry can be added to make the output voltage variable. The power delivered determines how bright and how much current each LED on the demo board will draw. With maximum brightness, the total current drawn by the LED board can be calculated by:

$$TotalCurrentDrawn = 5 \times .1A + 10 \times .04A = .9A \qquad (5.1)$$

■ 5.6 Charging Cellphone

After showing successful power transfer, the next step was to test the actual application. The application that this thesis is focusing on is wireless charging for cellphones. A similar setup to the LED demo, the transmitter board generates magnetic flux that is coupled onto the receiver board wirelessly. The receiver board rectifies and regulates the voltage to the 5V DC. The voltage regulator is integrated onto the same board as the receiver unit so that everything can operate from one PCB and fit inside the cellphone.
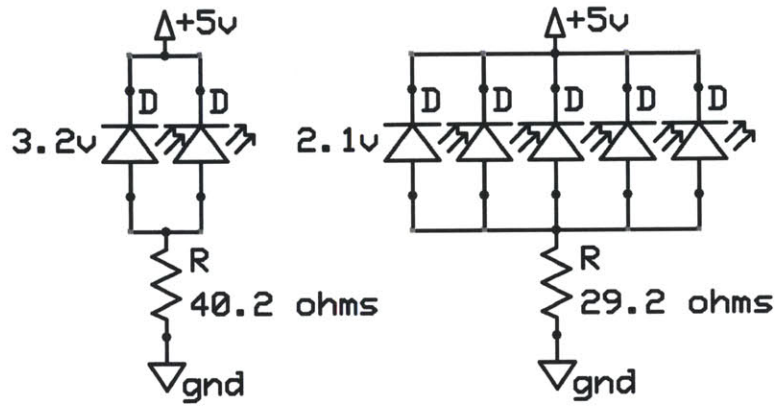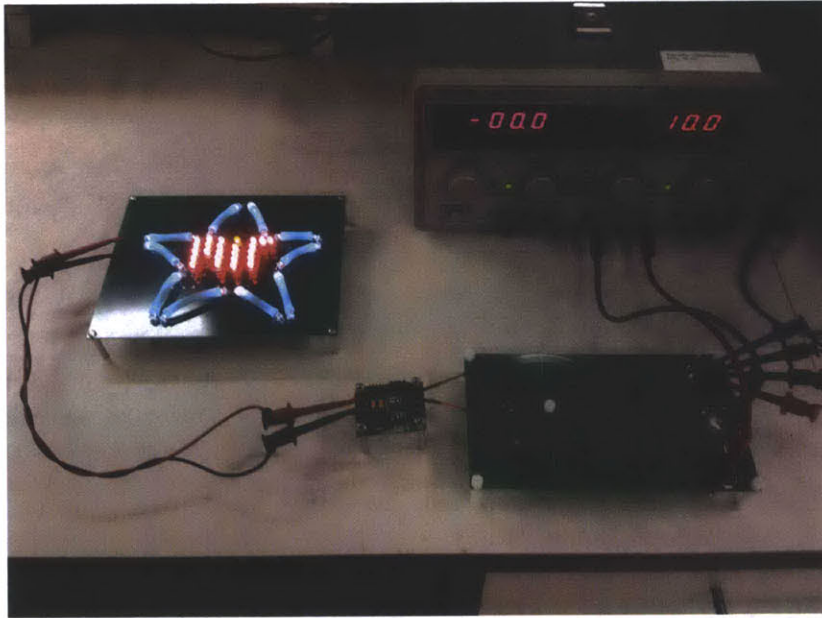
Figure 5.9: LED Demo Circuit

Figure 5.10: LED Demo

A USB to miniusb cable is used for connect the output to the phone during testing. As shown in Figure 5.11, when the system is turned on to the proper conditions, the cellphone can successful charge(the red light is on).
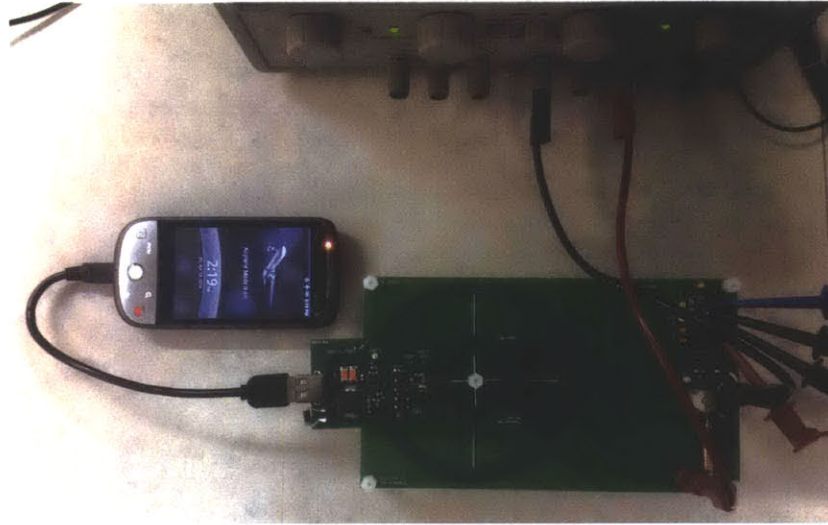
Figure 5.11: Charging Cellphone Demo

■ 5.7   Higher Frequencies

■ 5.8   6.78 MHz vs. 13.56 MHz Tradeoffs

Most commercial inductive wireless charging currently operate in the kHz range since there are more parasitics at higher frequencies. However higher frequencies are necessary if the system size is important. This thesis also explores the next ISM band, 13.56MHz, through simulations.

The main benefit of switching at higher frequencies is that since the components can be smaller, the overall converter size can also be reduced. Currently, the largest components are the primary and secondary coils. For the prototype boards implemented at 6.78MHz, the transmitter charging pad is 7x4inches and the receiver board that can be integrated into a cellphone is 1.7x2.8 inches. In Table 5.6 and Table 5.7, the potential decrease in coil sizes from 6.78MHz to 13.56MHz are shown. Data points with * are estimated actual parameters based on existing data. Actual coils were not implemented in these cases.

■ 5.8.1 Efficiency Comparisons

As the operating frequency increases, the parasitic capacitances of the transistor get charged up and discharged more frequently. Thus, the gate charge loss starts to dissipate

Table 5.6: Primary Coil Designs 6.78MHz vs. 13.56MHz

	TX #1	TX #2
Operating Frequency(MHz)	6.78	13.56
Outer Radius(mm)	46	25
Width(mm)	0.8	1.5
Height(mm)	0.036	0.036
Spacing(mm)	0.8	1
InnerRadius(mm)	40	15
Number of Turns	4	4
Inductance Real/Simulated (μF)	3.6/2.9	1*/.82
Resistance Real/Simulated(Ω)	2.5/0.8	0.9*/0.2
Quality Factor Real/Simulated (Q)	105/255	94*/395

Table 5.7: Secondary Coil Designs 6.78MHz vs. 13.56MHz

	RX #1	RX #2
Operating Frequency(MHz)	6.78	13.56
Outer Radius(mm)	18	9
Width(mm)	1	0.5
Height(mm)	0.036	0.036
Spacing(mm)	1	1
InnerRadius(mm)	10	5
Number of Turns	4	4
Inductance Real/Simulated (μF)	.79/.6	.2*/.2
Resistance Real/Simulated(Ω)	0.3/0.2	.4*/0.2
Quality Factor Real/Simulated (Q)	166/125	94*/126

more power.

$$P_{gateloss} = Q_G \times V_{in} \times f_{sw} \qquad (5.2)$$

From Figure 5.12, we can see that the MOSFET gate loss is almost the same as the conduction loss at 13.56MHz. However, the GaNFET gate loss is still much smaller than the conduction loss. Although at 6.78MHz, the gate losses for the MOSFET were

Breakdown of Losses on Transmitter Side (k=.1)

Source of Loss	MOSFET System		GaNFET System	
Gate Drive	44%	$\left.\begin{array}{c}\\\\\\\end{array}\right\rbrace$ Switch$_{Loss}$ =1.2W	11%	$\left.\begin{array}{c}\\\\\\\end{array}\right\rbrace$ Switch$_{Loss}$ =0.6W
Conduction	48%		84%	
Output Capacitance	8%		4%	

Figure 5.12: Inductive Charging System

still more than those of the GaNFET, but the differences are more significant at higher switching frequencies. The increase in gate losses results in the overall transistor losses in the MOSFET system to be double of the GaNFET system.

As the transistor losses become more significant, the overall system efficiency also suffers. Table 5.8 shows the system efficiencies for both systems as well as the differences in efficiencies based on simulations. The third column compares the differences in system efficiencies for the two switching frequencies.

Analysis of breakdown of losses are shown in Figure 5.13. The percentage of total power loss that the GaNFET transistor takes up is only 3% more going from 6.78MHz to 13.56MHz. However, in the MOSFET case, the contribution from the transistor loss increases by 11% based on simulations. This is consistent with the analysis that the transistor losses are more significant at higher frequencies due to intrinsic parasitics.

Table 5.8: Overall System Efficiency Comparison in Simulations

Coupling Coefficient (k)	GaNFET System 13.56MHz/6.7MHz)	MOSFET System (13.56MHz/6.7MHz)	Reduction in Losses (13.56MHz/6.7MHz)
0.6	39%/45%	29%/40%	10%/5%
0.8	50%/56%	41%/51%	9%/5%
0.1	57%/63%	49%/58%	8%/5%

GaNFET System Losses
k=0.06 at 6.78 MHz

■ TX Coil ■ RX Coil ■ Rectifier ▇Switch ■ RF Choke

GaNFET System Losses
k=0.06 at 13.56 MHz

■ TX Coil ■ RX Coil ■ Rectifier ▇Switch ■ RF Choke

(a)

(b)

MOSFET System Losses
k=0.06 at 6.78 MHz

■ TX Coil ■ RX Coil ■ Rectifier ▇Switch ■ RF Choke

MOSFET System Losses
k=0.06 at 13.56 MHz

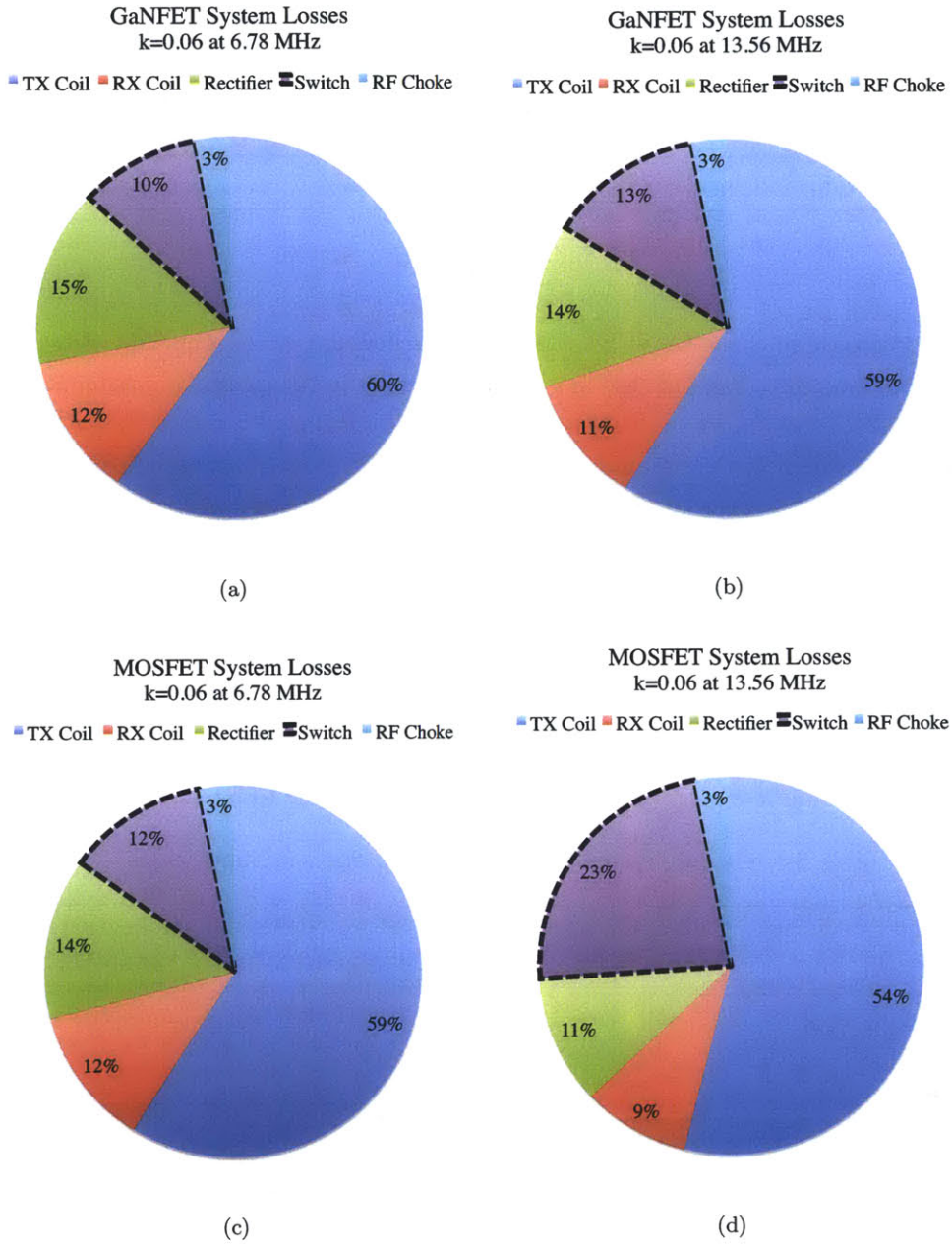■ TX Coil ■ RX Coil ■ Rectifier ▇Switch ■ RF Choke

(c)

(d)

Figure 5.13: Comparison of Breakdown of Losses for different frequencies at k=0.06

Chapter 6

Conclusion

■ 6.1 Conclusion

Although wireless charging technology continues to grow because of the convenience, it is important that the technology can stay environmentally friendly. There are many diverse applications to wireless charging, but they all face the same issue. Although wireless charging techniques may not surpass the efficiency of traditional wired charging methods, the end-to-end efficiency of wireless systems can definitely be improved. These inefficiencies of the wireless system are caused by the losses in the conversion circuits. This thesis focuses on improving one of the five main sources of loss: the transistor loss. This work attempts to improve the system efficiency by replacing the traditional Silicon MOSFET in most existing systems with a GaNFET. Since GaNFETs have much lower transistor parasitic resistance and capacitances than GaNFETs, there is the potential for system efficiency gain.

In this thesis, the magnetic resonant wireless systems implemented for 6.78MHz show that there is a 5% efficiency gain when implementing the GaNFET as the switch instead of the MOSFET. As Gallium Nitride technology continues to grow and expand, hopefully GaNFETs can become the main power switch in many more wireless charging applications.

■ 6.2 Future Work

The GaNFETs used in this thesis were commercial components (EPC2012). Since Gallium Nitride technology is continuing to improve and expand, it would be interesting to test the GaNFETs currently developed in research in the same system and compare the overall efficiency.

Other future work would include implementing the wireless charging systems at

even higher frequencies such as 13.56MHz. Though simulation results were shown in this thesis, actual efficiency results and converter size can vary. By going to higher frequencies, since the coils will physically be smaller, and there could be less unwanted coupling from the coils. In order to achieve ZVS to optimize efficiency until changing conditions, it would also be useful to incorporate a control loop into the system.

Chapter 7

Appendix

■ 7.1 Class A,B,C: Conduction Mode Power Amplifiers

Class A power amplifiers are the most basic. The basic topology consists of a RF choke (RFC) and a transistor. The RFC provides constant current into the transistor that is biased such that it operates in the saturation region during the entire cycle. Since the transistor is drawing current 100% of the duty cycle and the voltage and current are always positive, there is always power dissipation. Although Class A amplifiers benefit from high linearity, it comes at the cost of the efficiency. The maximum theoretical efficiency is about 50% [27]. The wasted power also needs to be removed with heat sinks.

Class B power amplifiers are better than Class A amplifiers in terms of efficiency with a reduction in linearity. In Class B amplifiers, the transistor only conducts current during 50% of the duty cycle. The transistor is biased at the threshold voltage so that half the time the transistor is in cut off and half the time in saturation. Since power dissipation is now only during half the cycle, there is an improvement in efficiency. However, the maximum theoretical efficiency is still only about 78% [27].

From Class A and Class B power amplifiers, there is clearly a tradeoff between efficiency and linearity. The conduction angle which is set by the biasing conditions directly impact the efficiency of the power amplifier. In order to get even higher efficiency, the power amplifier can conduct less than 50% of the duty cycle, such as in Class C power amplifiers which can attain 100% efficiency in theory but at zero P_{out}.

■ 7.2 Layout and Testing Techniques

Besides the circuit design, there are also layout and testing considerations to take into account. There are many issues that one can encounter when implementing an

actual wireless charging system.The main issues faced when implementing the systems, the cause of the issue, and solutions that were implemented in board revisions are discussed. The final layout of the transmitter and receiver board are shown in Figure 7.1 and Figure 7.2. An example of a good test setup used is shown in Figure 7.3.

■ 7.3 Potential Issues

1) Issue: Ringy input into Transistor

  Cause: Long Traces, parasitic L and C from trace cause oscillations

  Solution: Reduce trace length or add a resistor to dampen oscillations

  2) Issue: Unwanted Coupling from Coils

  Cause: Magnetic Field generates by primary coil and secondary can interfere with surrounding circuitry

  Solution: Reduce size of coils so magnetic field is more confined and try to move coil as far away from the rest of circuit as the size constraints allows

  3) Issue: Dealing with Sensitivity of Class E Power Amplifier

  Cause: Small changes in components values in Class E PA can greatly affect the amplifier efficiency and power delivered

  Solution: Use adjustable components to tweak until system is optimized

  4) Issue: Capacitance Losses

  Cause: Real capacitors have intrinsic resistance

  Solution: Use ceramic high Q, low ESR capacitors

  5) Issue: Oscilloscope Probes Coupling into System

  Cause: Capacitances of oscilloscopes can couple into system if magnetic field is large

  Solutions: Minimize loops of oscilloscope probes near the circuit
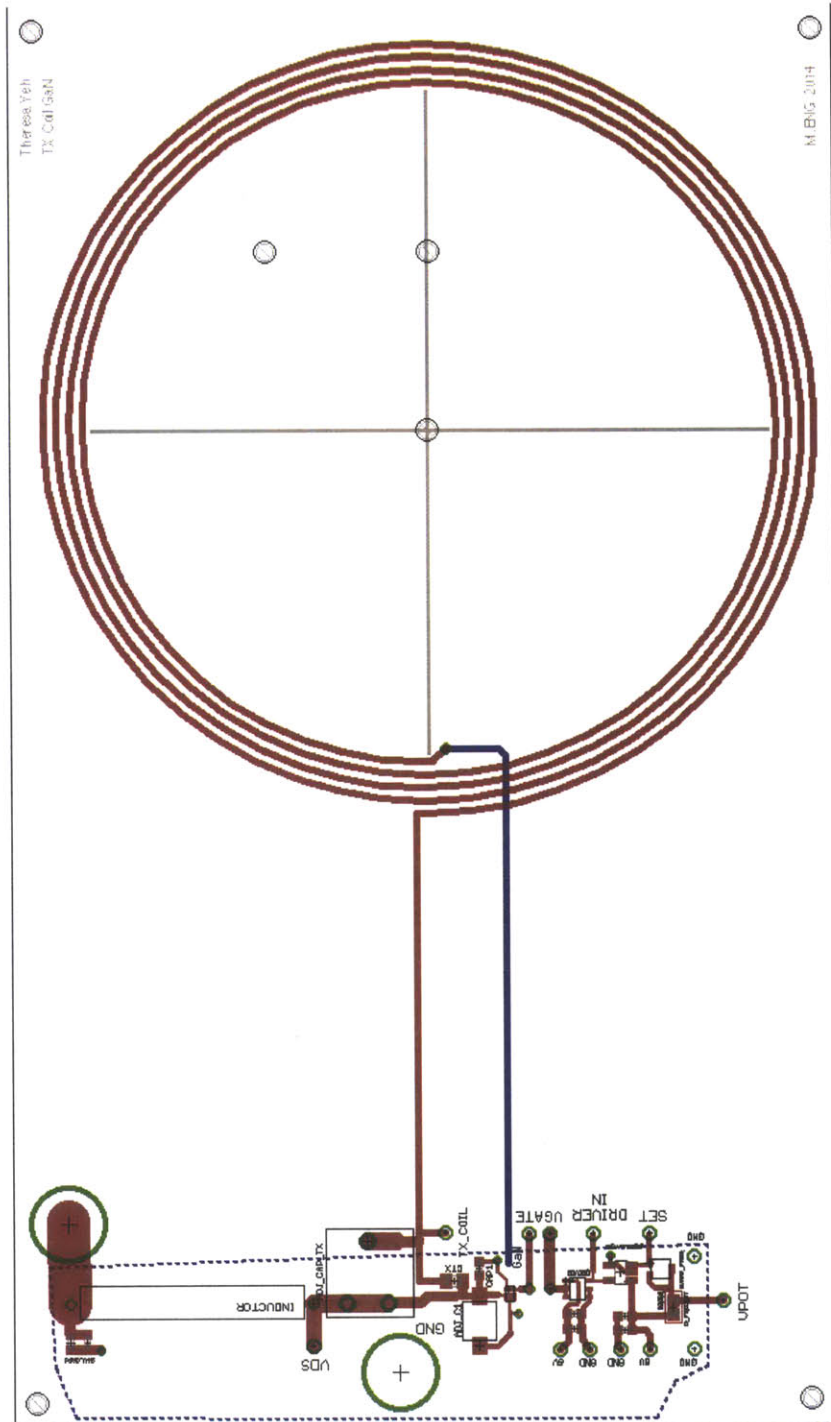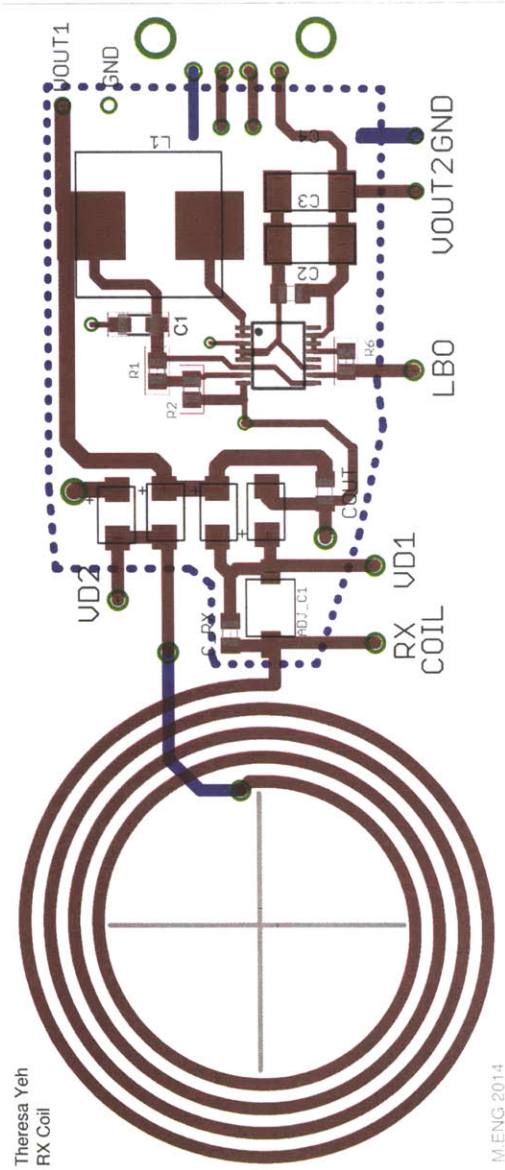
Figure 7.1: Transmitter Board with GaNFET

Figure 7.2: Receiver Board

Figure 7.3: Setup for Testing Efficiency

Bibliography

[1] Saad Al-Shahrani. *Design of Class-E Radio Frequency Power Amplifier.* PhD thesis, Virginia Polytechnic Institute and State University, 2001. 39

[2] M.W. Baker and R. Sarpeshkar. Feedback analysis and design of rf power links for low-power bionic systems. *Biomedical Circuits and Systems, IEEE Transactions on,* 1(1):28–38, March 2007. 33

[3] T. Bogoda. Adaptive primary side control for a wireless power transfer optimization. Master's thesis, Massachusetts Institute of Technology, 2012. 22

[4] Beach R. Colino, S. Fundamentals of gallium nitride power transisters. *EPC-Efficient Power Conversion Corporation,* 2009. 19

[5] Federal Communications Commision. Title 47, part 18 -industrial, scientific, and medical equipment. 29

[6] G.A. Covic and J.T. Boys. Inductive power transfer. *Proceedings of the IEEE,* 101(6):1276–1289, June 2013. 20

[7] Crown. Health effects of electric and magnetic fields. *Public Heaht England,* 2013. 20

[8] Jesus del Alamo. Schottky diode and ohmic contact. University Lecture, 2013. 11, 27

[9] EPC. Epc2012-enhancement mode power transistor. Oct 2012. 13, 19

[10] Jordi Everts, Jo Das, Jeroen Van dan Keybus, Marianne Germain, and Johan Driesen. Gan-based power transistors for future power electronic converters. In

Young Researchers Symposium 2010 on Smart Sustainable Power Delivery: Proceedings, 2010. 19

[11] Fairchild. Fds2670-200v n-channel powertrench mosfet. Aug 2001. 13, 19

[12] N. Garcia. Determining inductor coil losses. *Coilcraft*, 2005. 23, 24

[13] R. Jin. Circuits and systems for efficienct portable-to-portable wireless charging. Master's thesis, Massachusetts Institute of Technology, 2014. 41

[14] Tsuk J. Kamon, M. and J. White. Fasthenry, a multipole-accelerated 3-d-inductance extraction program. *Proceedings of the ACM/IEEE Design Automation Conference*, 1993. 32

[15] M. Kesler. Highly resonant wireless power transfer: Safe efficient, and over distance. *Witricity*, 2013. 16, 22

[16] B. Klug. Samsung Galaxy S4 Qi wireless charging pad and cover. *AnandTech*, 2013. 16

[17] D Krausse, F Benkhelifa, R Reiner, R Quay, and O Ambacher. Algan/gan power amplifiers for ism applications. *Solid-State Electronics*, 74:108–113, 2012. 19

[18] Andr Kurs, Aristeidis Karalis, Robert Moffatt, J. D. Joannopoulos, Peter Fisher, and Marin Soljai. Wireless power transfer via strongly coupled magnetic resonances. *Science*, 317(5834):83–86, 2007. 20, 22

[19] T. Lee. *The Design of CMOS Radio-Frequency Integrated Circuits*. Cambridge University Press, 2004. 36, 37, 42

[20] Wuhua Li and Xiangning He. Review of nonisolated high-step-up dc/dc converters in photovoltaic grid-connected applications. *Industrial Electronics, IEEE Transactions on*, 58(4):1239–1250, April 2011. 46

[21] QiBox. What is qi? 2013. 16

[22] F.H. Raab. Idealized operation of the class e tuned power amplifier. *Circuits and Systems, IEEE Transactions on*, 24(12):725–735, Dec 1977. 41

[23] R. Sarpeshkar. *Ultra Low Power Bioelectronics*. Cambridge University Press, 2010. 33

[24] N. Sokal. Class-e rf power amplifers. *QEX Commun*, 2001. 39

[25] N.O. Sokal and A.D. Sokal. Class e-a new class of high-efficiency tuned single-ended switching power amplifiers. *Solid-State Circuits, IEEE Journal of*, 10(3):168–176, Jun 1975. 39

[26] D. Wageningen and E. Waffenschimidt. Inductive power transmission. *Wireless Power Consortium*, 2011. 11, 15, 21

[27] H. Wai. A 1-v cmos power amplifier for bluetooth applications. Master's thesis, Hong Kong University of Science and Technology, 2002. 11, 37, 40, 69

[28] Patrick Waltereit, Richard Reiner, Heiko Czap, Detlef Peschel, Stefan Müller, Rüdiger Quay, Michael Mikulla, and Oliver Ambacher. Gan-based high voltage transistors for efficient power switching. *physica status solidi (c)*, 10(5):831–834, 2013. 19

[29] Wikipedia. Power mosfet, 2014. [Online; accessed May 2014]. 11, 25